TWELFTH INTERNATIONAL CONFERENCE ON
ELECTRICAL MACHINES, DRIVES AND POWER SYSTEMS

ELMA 2008

16 – 18 October 2008, Sofia, BULGARIA

PROCEEDINGS

Volume 2

Supported by: IEEE Bulgaria Section

VDE

Organised by:

Union of electronics, electrical engineering
and telecommunications (CEEC) – EUREL Member
Technical University of Sofia
Technical University of Varna
Technical University of Gabrovo
University of Rousse

ELMA 2008 – XII International Conference on Electrical Machines, Drives and Power Systems

16 – 18 October 2008, Sofia, BULGARIA

Proceedings

Editorial board: Gancho Bojilov, Dimitar Sotirov, George Todorov, Zahari Zarkov

Printed by AVANGARD, Sofia, Bulgaria

Number of copies: 150

Printing of this edition has been financially supported by
The Technical University of Sofia

ISSN 1313-4965

These Proceedings are reviewed by members of The Program Committee.

ELMA 2008 is supported also by:

- ELPROM TRAFO CH Kyustendil
- SPARKY ELTOS Lovech
- ELPROM – ZEM Sofia
- ELDOMINVEST Varna
- DENIMA Sofia
- ABB-Avangard Sevlievo
- HYUNDAY Heavy Industries
- ELMOT Veliko Tarnovo
- DIT-M Sofia
- MMOTORS Etropole
- CERB Sofia
- Prof. Gancho Bojilov and Yassen Bojilov
- PRIOR Sofia
- ZAVN Dobrich
- ELECTROINVENT Sofia
- ELPROM – IEP
- ELPROM – ILEP
- TROYAN MOTOR
- INOVATICS Sofia
- DENI-EN-K Sofia
- ELISOT Sofia
- DNT Varna, Plovdiv, Bourgas, Rousse

STEERING COMMITTEE

CONFERENCE CHAIRMEN

Gancho BOJILOV	CEEC
Dimitar SOTIROV	Technical University of Sofia

ORGANIZING COMMITTEE

Chairman:

Vladimir LAZAROV	Technical University of Sofia, Bulgaria

Secretariat:

Ivan VASSILEV	CEEC, Bulgaria
George TODOROV	Technical University of Sofia, Bulgaria
Zahari ZARKOV	Technical University of Sofia, Bulgaria
Yuli STAFUNSKI	Technical University of Varna, Bulgaria

INTERNATIONAL PROGRAM COMMITTEE

Viktor BESPALOV – Technical University – Moscow, Russia
Stanislaw BOLKOWSKY – SEP, Warsaw, Poland
Gerard-Andre CAPOLINO – Université de Picardie, France, Chair of ICEM
Milan CHUNDEV – University " Sts. Cyril & Methodius", Skopie , Macedonia
Manuel Perez DONSION – Vigo University, Spain
Gerhard DREGER – VDE – Frankfurt, Germany
Pancho DUNDAROV – CEEC, Bulgaria
Masato ENOKIZONO – Oita University, Japan
Bulent ERTAN – Middle East Technical University, Ankara, Turkey
Ionescu FLORIN – UPB Bucharest , Romania
Bruno FRANCOIS – Ecole Centrale – Lille, France
Antonios KLADAS – NTUA , Greece
Afef LEBOUC – LEG – INPG, France
Jiri LETTL – CVUT – Prague, Czech Republic
Gerard MEUNIER – LEG – INPG, France
Emil MITEV – Polytechnic Radom, Poland
Gilles NOTTON – Université de Corse, France
Lidija PETKOVSKA – University " Sts. Cyril & Methodius", Skopie , Macedonia
Viktor PETROUSHIN – Odessa Polytechnic Institute, Ukraine
Michel POLOUJADOFF – Université Pierre et Marie Curie, Paris, France
Ioan POPA – University of Craiova, Romania
Viktor POPOV – Technical University of St. Petersbourg, Russia
Mircea RADULESKU – Technical University of Cluj-Napoca, Romania
Saifur RAHMAN – Virginia Tech, USA
Christian SCHAEFFER – LEG – INPG, France
Wolfgang SCHROPPEL – Technical University of Chemnitz, Germany
Sergey SHIRINSKY – Technical University – Moscow, Russia
Emil SOKOLOV – Technical University, Sofia, Bulgaria
John TEGOPOULOS – NTUA, Greece
Christian VASSEUR – Université de Lille, France

NATIONAL PROGRAM COMMITTEE

Alexander ALEXANDROV - Technical University of Sofia
Rumen ATANASOV – BCEE
Lyubomir BALGARANOV - Technical University of Sofia
Ivelin BUROV - BDS
Dimitar DIMITROV - Technical University of Varna
Peter DINEFF - Technical University of Sofia
Nikolai DJAGAROV - Technical University of Varna
Valentin FILIPOV – ZEM Sofia
Vasil GOSPODINOV - Technical University of Sofia
Nikola GRADINAROV - Technical University of Sofia
Stefcho GUNINSKI - Technical University of Sofia
Marin HRISTOV - Technical University of Sofia
Kostadin ILIEV - Technical University of Sofia, branch Plovdiv
Todor IONKOV - Technical University of Sofia
Dimitar JETCHEV - Technical University of Sofia
Anatoli IVANOV – SPARKY Eltos
Nikola KALOYANOV - Technical University of Sofia
Maria KANEVA - Technical University of Sofia
Yordan KOLEV – IEEE Bulgaria section
Sava KONTROV - Technical University of Varna
Anastasia KRASTEVA - Technical University of Sofia
Iliana MARINOVA - Technical University of Sofia
Maria MARINOVA - Technical University of Varna
Deshka MARKOVA - Technical University of Gabrovo
Alexandar MAVRODIEV – CERB Sofia
Nikolai MICHAILOV – Rousse University
Miho MIHOV - Technical University of Sofia
Mincho MINCHEV - Technical University of Sofia
Petar NAKOV - Technical University of Sofia
Petko NOTOV - Technical University of Sofia
Ivaylo PANAYOTOV – Elprom Trafo SN Kyustendil
Angel PACHAMANOV - Technical University of Sofia
Lazar PETKANCHIN - Technical University of Sofia
Petar PETROV – INOVATIX
Encho POPOV – DENI-EN Ltd
Emil RATZ - Technical University of Sofia
Plamen RIZOV - Technical University of Sofia

Georgi SAVOV - ELPROM Harmanli

Stanimira SHISHKOVA - Technical University of Sofia, branch Plovdiv

Nikola SHOYLEV – UCTM Sofia

Yordan SHOPOV - Technical University of Sofia

Rumiana STANCHEVA - Technical University of Sofia

Stefan TABAKOV – Technical University of Sofia

Ivan TZANKOV – ELMOT Veliko Tarnovo

Slavka TZANOVA – Technical University of Sofia

Raina TZENEVA - Technical University of Sofia

Angel TZOLOV – Technical University of Sofia

Hristo VASSILEV - Technical University of Sofia

Petko VITANOV - Bulgarian Academy of Sciences

Pencho VLADIMIROV - Technical University of Gabrovo

Ivan YATCHEV - Technical University of Sofia

Kiril ZAHARINOV - Technical University of Sofia

TABLE OF CONTENTS

POSTERS

Power transmission system state estimation during conditions of voltage instability using power transfer efficiency

Rad Stanev

Abstract: *In this paper power transfer efficiency is defined and proposed to be used as an indicator for estimation of the transmission system state during conditions of voltage instability. A simple two-bus system is used to demonstrate the approach. The indicator proposed is extremely evident having the essential advantage of staying close to the physical nature of the problem. Its simple numerical calculation makes it favorable both for off-line or on-line, power flow or direct measurement based applications. Comparison with other voltage stability indices is made and valuable conclusions are drawn.*

Keywords: *voltage stability, power transfer efficiency, state estimation methodology, steady-state voltage stability, voltage collapse*

Introduction

Voltage stability has become a major concern for many power systems during the recent decade. Many indicators for voltage stability analysis have been developed and presented in previous papers [1,2,3,4]. One of the most important issues of the voltage stability problem consists of the inability of the power system to deliver power to the unstable area. In this paper a new branch oriented indicator is proposed in order to show the transmission system state during voltage instability.

Methodology

One of the important factors leading the system to voltage instability is the inability of the power system to transfer active and reactive power to the emerging load area. When the load in the area is increased, the losses in the transmission system elements which are connecting this area to the electrical power system grow significantly [4]. Thus after the critical voltage collapse point is reached the stability is lost and the transfer element figuratively said gets "stuck".

Focusing on this fact the *power transfer efficiency* is proposed to be used as a voltage stability indicator.

For any branch of the transmission system connecting busses i and j the power transfer efficiency (PTE) can be defined as a ratio between the received power and the sent power (Fig. 1):

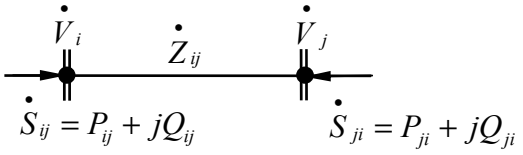

Fig.1.One line diagram for a particular branch of the power system.

$$PTE_{ij} = \left| \frac{\min(\dot{S}_{ij}, \dot{S}_{ji})}{\max(\dot{S}_{ij}, \dot{S}_{ji})} \right| . \quad (1)$$

Since the power transferred is a complex number, real and reactive power transfer efficiencies can be defined:

$$realPTE_{ij} = \left| \frac{\min(P_{ij}, P_{ji})}{\max(P_{ij}, P_{ji})} \right| \quad (2)$$

and

$$reactivePTE_{ij} = \left| \frac{\min(Q_{ij}, Q_{ji})}{\max(Q_{ij}, Q_{ji})} \right| . \quad (3)$$

Considering the complex powers $\dot{S}_{ij}$ and $\dot{S}_{ji}$ which are flowing through the branch enclosed between nodes i and j, the power losses can be easily obtained:

$$\Delta \dot{S}_{ij} = \dot{S}_{ij} + \dot{S}_{ji} = (P_{ij} + P_{ji}) + j(Q_{ij} + Q_{ji}) . \quad (4)$$

Branch with power transfer efficiency close to 1 presents normal operation with small power losses. When the power losses in the branch become high a large amount of the energy injected in the branch is consumed from this branch instead of being transferred. Thus a branch with power transfer efficiency close to 0 presents abnormal and unstable operation.

Active and reactive power transfer efficiencies show the state of the transmission system and its elements indicating which the most overloaded branches are.

Power transfer efficiencies can be defined for a particularly chosen branch, for the transmission system of a selected area of the power system, or for the transmission system of the entire power system.

The indicator is extremely simple, evident and computationally inexpensive. The only variables needed for determining the power transfer efficiency are the powers $\dot{S}_{ij}$ and $\dot{S}_{ji}$ which are flowing through the branch. That is why this new voltage stability indicator can be easily evaluated on-line (based on direct measurements) or off-line (based on power flow computation) as well. For the off- line studies the power flow problem can be solved using the well known Newton- Raphson method or using some of its modifications which present better convergence properties close to the collapse point where the Jacobian of the power flow equations becomes singular.

After the unknown steady- state variables are found the powers $\dot{S}_{ij}$ and $\dot{S}_{ji}$ which are flowing through the line can be easily determined for example using the following well known equations [1,2]:

(5) $$P_i = \sum_{i \in j} V_i V_j (G_{ij} \cos\theta_{ij} + B_{ij} \sin\theta_{ij})$$

(6) $$Q_i = \sum_{i \in j} V_i V_j (G_{ij} \sin\theta_{ij} - B_{ij} \cos\theta_{ij})$$

where $\theta_{ij} = \theta_i - \theta_j$;

P_i and Q_i are the active and reactive power at bus *i.*

G_{ij} and B_{ij} are the mutual conductance and susceptance respectively between nodes *i* and *j;*

V_i and V_j are the voltages at bus *i* and *j* respectively;

θ_i and θ_j are the voltage angles at bus *i* and *j*.

Test results

In order to present the main properties of the new indicator a simple two bus power system will be considered (Fig 2).

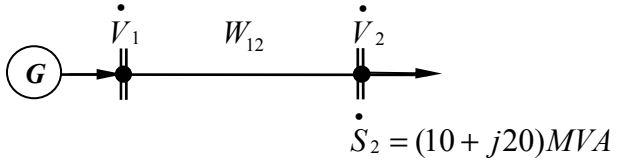

Fig.2. One line diagram of a two bus test system.

The system consists of two busses which are connected throughout the line W_{12}. The generator bus 1 is assumed as a slack bus whereas bus 2 is a load (PQ) bus. The complex impedance of the line W_{12} is:

(7) $$\dot{Z}_{12} = \dot{Z}_{21} = 0{,}12 + j0{,}16\, p.u.$$

on $S_{base} = 100MVA$. The complex load power at bus 2 consumed in the initial steady state is:

(8) $$\dot{S}_2 = P_2 + jQ_2 = (20 + j10)MVA$$

More detailed description of the test system is given at [5]. A static voltage stability analysis is performed using the ***STATUS*** power system analysis software [4]. The system is stressed until the critical, voltage collapse point is reached. Although the unstable (low voltage) solutions of the power flow equations basically do no not present any significant practical interest, for this simple theoretical example the evaluation of the low voltage solutions gives a good opportunity for extensive research of the main properties of the new indicator. That is why some special modifications of the Newton- Raphson method based on the "*prediction- correction*" technique [2] are used in order to obtain the unstable power flow solutions. For verification and evaluation of the features of the new indicator proposed some other well known and proven voltage stability indices already described in [4] will be shortly considered. Table 1 presents numerical values of the voltage stability indices at three typical points:

- Point A corresponds to normal light load stable operation in initial steady state at $\dot{S}_2 = (20 + j10)MVA$
- Point B corresponds to the critical voltage collapse point at $\dot{S}_2 = (132{,}6 + j66{,}3)MVA$.
- Point C corresponds to unstable operation point at $\dot{S}_2 = (20 + j10)MVA$

Table 1

Voltage stability indicators

Indicator	Point A	Point B	Point C
V, p.u.	1,0206	0,5446	0,0438
VQ Sensitivity	0,1608	∞	-0,0945
Min Eigvalue	6,2179	0	-10,5776
$\Delta P, MW$	0,57	88,89	312,50
$\Delta Q, MVA$	0,76	118,62	416,67
$PSM, \%$	84,9	0	-
real PTE	0,9720	0,5985	0,0602
reactive PTE	0,9287	0,3586	0,0234

- V-P and V-Q curves

Figure 3 shows the V-P and V-Q curves for the system examined. The points in the upper part of the V-P and V-Q curves are stable. At the critical point, at which the transferred power is maximal, the voltage at bus 2 is 0,54 and system is at the verge of stable state [1,2,3]. Considering the loading distance between initial and critical steady state the percent stability margin PSM can also be used as a measure of the proximity to instability [2]:

$$PSM = \frac{P_{\max} - P_0}{P_{\max}}.100\%$$

For this particular system the percent stability margin is 84,9 % which presents a good stability reserve in the initial steady state.

- V-Q Sensitivity (VQS) [2]

V-Q sensitivity at bus 2 defines the slope of the Q-V curve for this bus when calculating the pseudo steady state. The small and positive VQ sensitivity of 1,02 at point A witnesses stable steady state. With decreasing the stability, the sensitivity grows, reaching infinity at the verge of stability at point B (Fig. 4). Negative V-Q sensitivity of -0,09 at point C is an indication of unstable operation [2,4].

- Q-V Modal analysis [2,4]

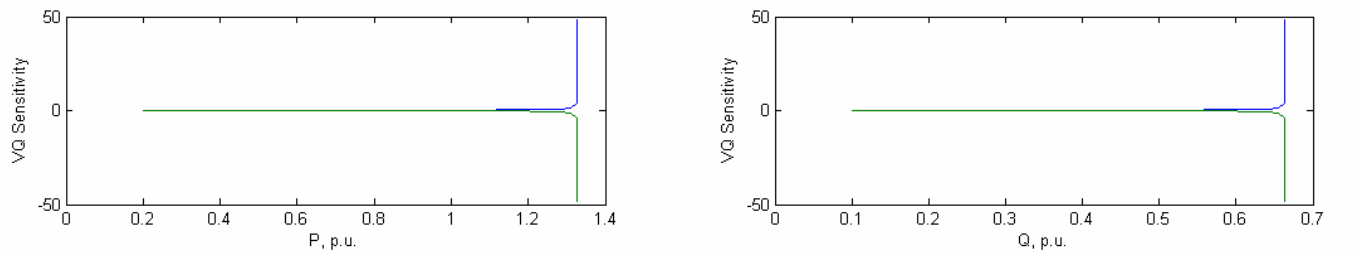

Fig.4. V-Q Sensitivity at bus 2.

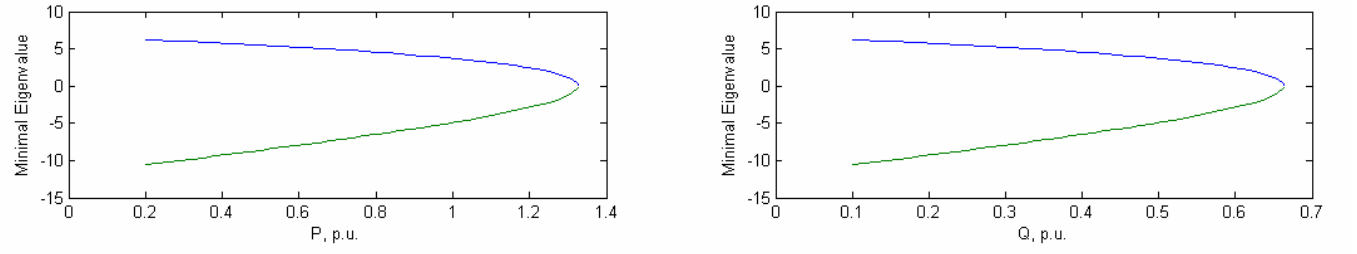

Fig.5. Minimal eigenvalue.

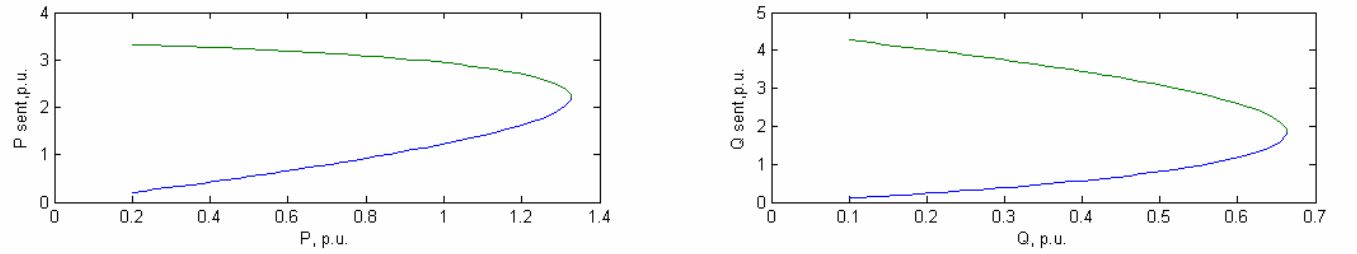

Fig.6. Sent active and reactive power.

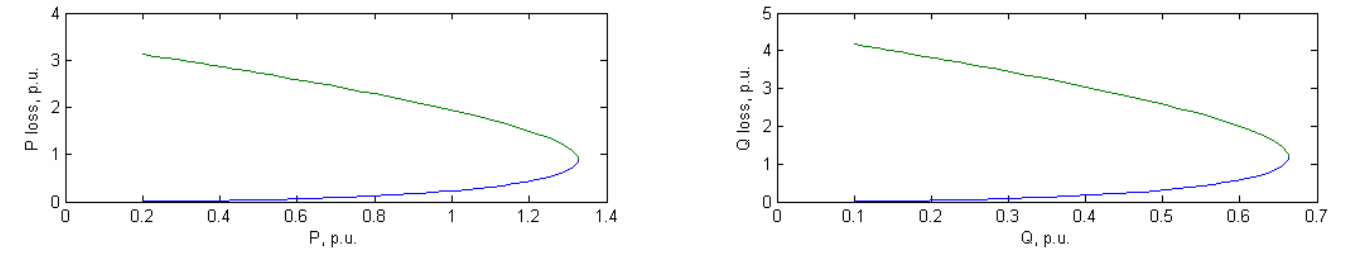

Fig.7. Active and reactive power loss.

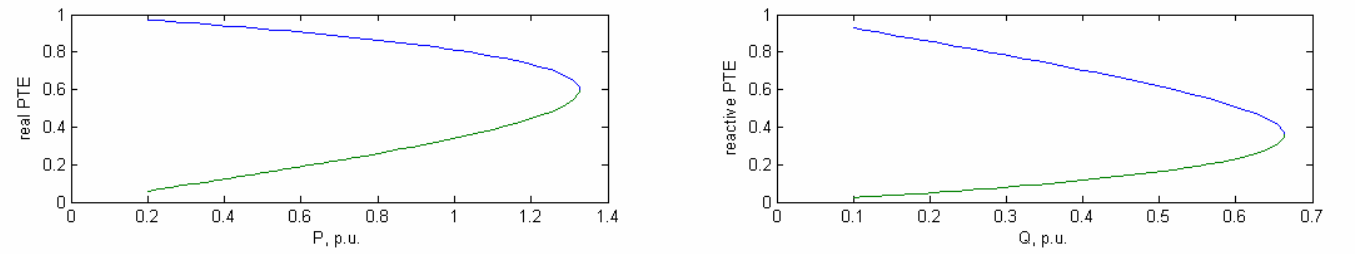

Fig.8. Real and reactive power transfer efficiency.

The magnitude of the i^{th} eigenvalue determines the degree of stability of the i^{th} modal voltage. The smaller the magnitude of positive, the closer the i^{th} modal voltage is to being unstable. At point A (fig. 5) the minimal eigenvalue is 6,2 indicating that the system is voltage stable. At the critical point B the minimal eigenvalue is equal to 0 showing that the system is on the verge of stability. The negative eigenvalue of -10,58 at point C witnesses unstable operation.

- Power loss

The real power loss ΔP at the stable operation point A takes an approximately small value (0,57 MW) (fig. 7) and the sent power is almost equal to the received power (fig. 6). When the operation point approaches the voltage stability limit the real power loss increases reaching 88,9 MW at the critical point B. At the unstable point C the real power loss is 312,5 MW which is almost equal to the sent power. For this unstable operation point almost all the power amount sent is lost in the line. The reactive power loss shows similar behaviour to the active power loss (fig. 7). The only difference which can be observed between active and reactive power loss is that the reactive power loss seems to be more sensitive to the voltage stability decrease.

- Power transfer efficiency

At the stable point A the value of the real power transfer efficiency is 0,97 which is close to 1 (fig.8). At the critical point B the real power transfer efficiency is approximately 0,6. After the stability is lost the power transfer efficiency tends to 0 and at the unstable point C it is equal to 0,06.

Reactive power transfer efficiency shows similar properties to the real power transfer efficiency with the only difference that it is more sensitive to the voltage stability decrease (fig. 8). It is 0,93 at point A, 0,36 at point B and 0,02 at point C.

One disadvantage of the PTE is the fact that it does not take a typical value at the critical point and consequently it can not present clear information about the proximity of the system to voltage instability.

Unlike the V-P and V-Q curves, minimal eigenvalue, V-Q sensitivity and other well known indices, power transfer efficiency is not a property of a bus. It is likely focused on the state of the branches of the transmission system and in this way it shows the most overloaded branches in the system which are not able to transfer power effectively and for which remedial measures should be taken.

Similarly to the other indices already described, power transfer efficiency shows nonlinear behaviour.

Conclusion

The power transfer efficiency is defined and proposed to be used as an indicator of the transmission system state during conditions of voltage instability. A numerical example is presented in order to demonstrate the main properties of the new indicator after which a comparison with other well known indicators is made. The new indicator is simple and evident and promises to be useful for the estimation and analysis of the processes driving the power system to voltage instability. The main purpose of this indicator is not to determine the distance to voltage instability. Instead of this it shows the states of the branches of the complex large-scale electric power system, indicating the most overloaded branches in the system, which are not able to transfer power effectively.

References

[1] C. W. Taylor, "Power System Voltage Stability", McGraw-Hill, Inc., 1996.

[2] P. Kundur, "Power System Stability and Control", McGraw-Hill, 1994

[3] T. V. Cutsem, C. Vournas, "Voltage Stability of Electrical Power Systems", Kluwer Academic Publishers, 1998

[4] P. Notov, Stanev R., "Voltage stability- essence, methodology and analysis", Energetika Journal, No. 4, 2006

[5] http://www.tu-sofia.bg/Bul/faculties/ef/ee/index.htm

Biographies

Rad Stanev received his B.S. and M.S. degrees in Electrical Engineering from the Technical University of Sofia, Bulgaria in 2003 and 2005 respectively. In 2006 he received his Master of Business Administration (MBA) degree from FOM Essen Germany and the Faculty for German Engineering Education and Industrial Management at Technical University - Sofia, Bulgaria. Since July 2005 he is a PhD Student in the Power Engineering Department of Technical University – Sofia. His research interests are in the field of voltage stability, power systems analysis, renewable energy sources, liberalized electricity markets, management and control. Rad Stanev is with the Faculty of Electrical Engineering, Technical University of Sofia, 8, Kl. Ohridski Blvd., 1000 Sofia, Bulgaria (e-mail: rstanev@tu-sofia.bg).

A Rapid Torque Response DTC Approach via Improving Inverter Switching Pattern

Mehdy Khayamy, Sadegh Vaez-Zadeh
School of Electrical and Computer Engineering, University of Tehran , Iran
Email: m.khayamy@ece.ut.ac.ir, vaezs@ut.ac.ir

Abstrac: *Direct Torque Control (DTC) has appeared as a practical control scheme for AC motor drives with potential for fast dynamic performance. In this paper a combined switching pattern is proposed to improve torque response substantially.*

Keywords: DTC, Voltage Vector, Torque Dynamic, Switching pattern, Inverter

Introduction

Basic DTC scheme uses six voltage vectors to rotate the flux vector and consequently rotor itself. On the contrary, an alternate lookup table could be used to provide twelve nonzero voltage vectors by a conventional voltage source inerter. Effects of these new voltage vectors on the rapid performance of DTC are the primary concern of this paper.

Voltage Vectors of an Inverter

Since a conventional voltage source inverter has six switches and each switch has two states (On/Off), theoretically an inverter could have $2^6 = 64$ states but most of them are not acceptable due to DC-Link shorting and current loop problems. There are 15 useful states which lead to 15 equivalent voltage vectors including 3 zero voltages. Fig.1 describes an equivalent switch which could be used to model one of the inverter columns. Although this equivalent switch does not provide all the inverter column properties including free whell diode, but it is appropirate for this study. According to the equivalent switch, one phase of motor could be connected to $V_{DC}/2$, zero (float) or $-V_{DC}/2$.

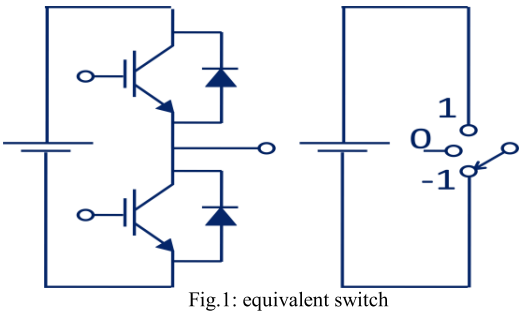

Fig.1: equivalent switch

Line to line voltages, could be written as:

$$u_{ab} = V_{DC}(S_A - S_B) \;,\; u_{bc} = V_{DC}(S_B - S_C)$$
$$u_{ca} = V_{DC}(S_C - S_A) \qquad (1)$$

Considering

$$u_a = (3u_a)/3 = [2u_a + (-u_b - u_C)]/3 \qquad (2)$$

phase voltages are:

$$u_a = (u_{ab} - u_{ca})/3 \;,\; u_b = (u_{bc} - u_{ab})/3$$
$$u_c = (u_{ca} - u_{bc})/3 \qquad (3)$$

With replacement of equation (1) into the (2), we will have:

$$u_a = V_{DC}\frac{(2S_A - S_B - S_C)}{3} \qquad u_b = V_{DC}\frac{(2S_B - S_A - S_C)}{3}$$
$$u_c = V_{DC}\frac{(2S_C - S_A - S_B)}{3} \qquad (4)$$

Space-phasor of voltage in case of 3phase motor is [1]:

$$\overline{U_s} = (2/3)\left(u_a + e^{j2\pi/3}u_b + e^{j4\pi/3}u_c\right) \qquad (5)$$

So Space-phasor of voltage could be rewritten as:

$$\overline{U_s} = V_{DC}\,(2/3)\left(S_A + e^{j2\pi/3}S_B + e^{j4\pi/3}S_C\right) \qquad (6)$$

Related to value of equivalent switches of each column, voltage vector could have different angle and amplitude.

six out of the twelve zon-zero voltage vectors ,group1, have the same amplitude. For these vectors all three equivalent switches are 1 or -1 (always one power switches in each inverter column is conducting). For example for $\overline{V_1}$ equivalent switches are (1, -1, -1) and the amplitude and angle are:

$$|\overline{V_1}| = \left|V_{DC}\left(\frac{2}{3}\right)\left(1 - e^{\frac{j2\pi}{3}} - e^{\frac{j4\pi}{3}}\right)\right| = V_{DC}\,(2/3) \times 2 \qquad (7)$$

$$< \overline{V_1} = V_{DC}\left(\frac{2}{3}\right) < \left(1 - e^{\frac{j2\pi}{3}} - e^{\frac{j4\pi}{3}}\right) = 0 \qquad (8)$$

Voltage angles of this group are (0 60 120 180 240 300) degrees. Vectors of group1 are used to appling to induction and synchronous motors DTC drive. Fig.2 shows the inverter states to generate $\overline{V_1}$,first vector of this group. As it is obvious, all three columns have a role in making this vector.

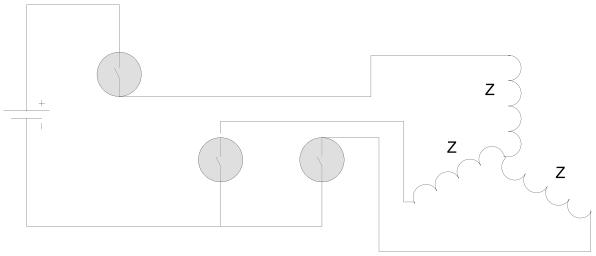

Fig.2: Equivalent circuit of applying vector 1

Other six nonzero voltages ,group2, have the same amplitude too. For these vectors one equivalent switche is 0 and the others are 1 and -1. For example for $\overline{V_2}$ equivalent switches are (1, 0, -1):

$$|\overline{V_{s2}}| = \left|V_{DC}\ \left(\frac{2}{3}\right)\left(1 - e^{\frac{j4\pi}{3}}\right)\right| = V_{DC}\ (2/3) \times \sqrt{3} \qquad (9)$$

$$< \overline{V_2} = V_{DC}\ \left(\frac{2}{3}\right) < \left(1 - e^{\frac{j4\pi}{3}}\right) = 30° \qquad (10)$$

Voltage angles of this group are (30 90 150 210 270 330) degrees. The second group which simultaneously uses two columns to generate a vector, used to drive a BLDC motor. Fig.3 shows the inverter states to generate $\overline{V_2}$ or the first vector of group2.

The ratio of these two groups amplitudes is $|\overline{V_{s1}}|/|\overline{V_{s2}}| = 2/\sqrt{3} = 1.154$ and each voltage of the first group is located between two vectors of the second group and vice versa as illustrated in fig.4

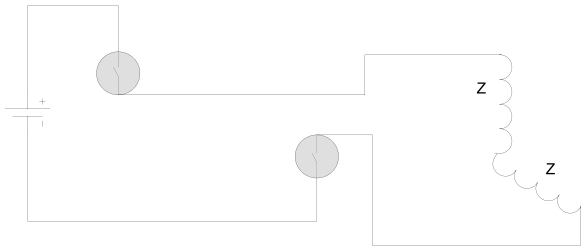

Fig.3: Equivalent circuit of applying vector 2

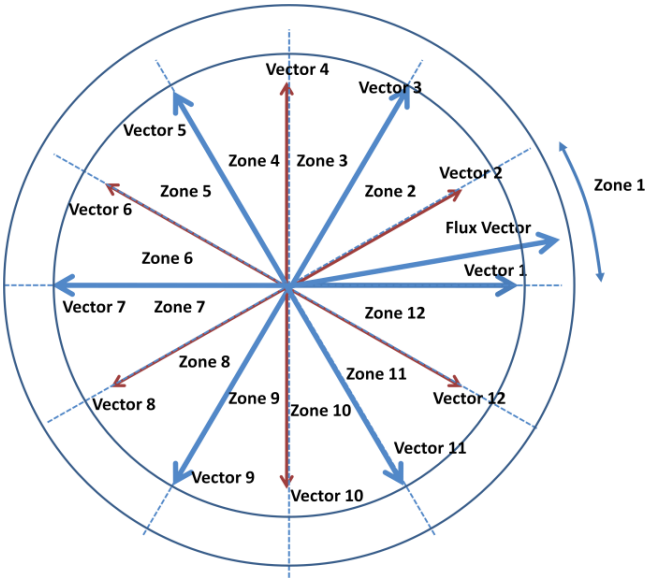

Fig.4: voltage vectors and zones

In the next section, these twelve voltage vectors will be used to produce an appropriate lookup table for achieving a rapid torque response.

Choosing Voltage Vectors For Rapid Torque

A voltage vector applied to an AC motor by a DTC system ,$\vec{V_s}$,could be decomposed into two components, where the first one is in the direction of the machine flux vector ,radial component, and the second component is perpendicular to the first one ,tangential component, as it is illustrated in Fig.3. It is known that the first component affects the flux magnitude and the second one influences on flux angle rotation and torque.

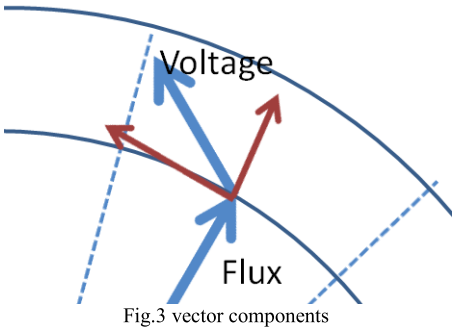

Fig.3 vector components

In a conventional DTC with six voltage vectors, in a specific zone, just a unique vector is applicable and the other vectors do not satisfy both flux and torque demands.

Using twelve voltage vector from a conventional inverter with the mention method, each of previous zones could be separated into two zones, so we have twelve zones (0-30˚, 30-60˚,…,330-360˚). Having twelve vector bring the opportunity to have a more choice in a specific zone and specific torque and flux hysteresis.

Two methods could be selected. In the first method ,which is an extend to six vector, those vectors will be selected to have approximately equal effect on torque and flux changes. For zone1 (0-30˚) four vectors which are appropriate for this method according to torque and flux hysteresis are depicted in table1. Torque and flux will have almost the same response as using six voltage vectors.

In the second method, those vectors will be selected that moreover that satisfy torque and flux hysteresis, have greater tangential component compare to radial component as depicted in the fast torque response of table1.

Table (1): zone 1 ,one part of lookup table

Zone1	Proposed direction
T ↕	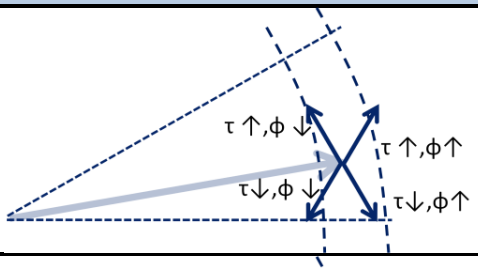
T ↑	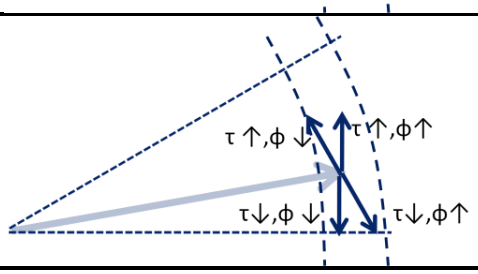

Tangential component of a voltage vector is a function of flux vector angle as described in Fig. 3. It is possible to plot vectors tangential components for all flux vector angles and it has sinusoidal shape. Fig. 4 illustrated the voltage vectors tangential component versus flux angle. This figure is plotted for the case of torque increment and for torque decrement it will be analogy. Conventional DTC approach uses only the odd vectors and in each zone selected vector will be switched among two vectors continuously to hold flux in the hysteresis band. As it could be seen in Fig. 4, even vector have smaller amplitude as Eq.2 described before.

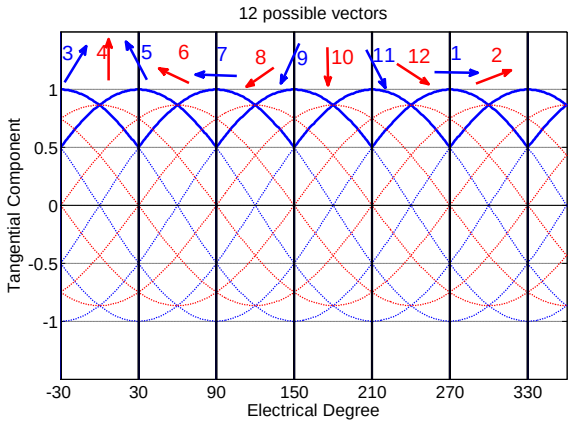

Fig.4. tangential components in conventional DTC

Average applied vector tangential components could be derived as Eq. 3. Although this Eq. is calculated for zone, due to symmetry other zones have the same value.

$$V_{t\ ave} = \frac{0.5}{\pi/6}\left[\int_0^{\pi/6} sin\left(x+\frac{\pi}{3}\right)dx + \int_0^{\pi/6} sin\left(x+\frac{2\pi}{3}\right)dx\right] = 0.827 \quad (3)$$

Fig.4 shows that with considering other six vectors, there is opportunity to increase average applied vector tangential components as it illustrated in Fig. 5. Computation of average tangential value in Eq. 4 demonstrates that using this switching method will results in at least 7.735% improvement.

$$\frac{0.5}{\pi/6}\left[\int_0^{\pi/6} sin\left(x+\frac{\pi}{3}\right)dx + \frac{\sqrt{3}}{2}\int_0^{\pi/6} sin\left(x+\frac{\pi}{2}\right)dx\right] = 0.891 \quad (4)$$

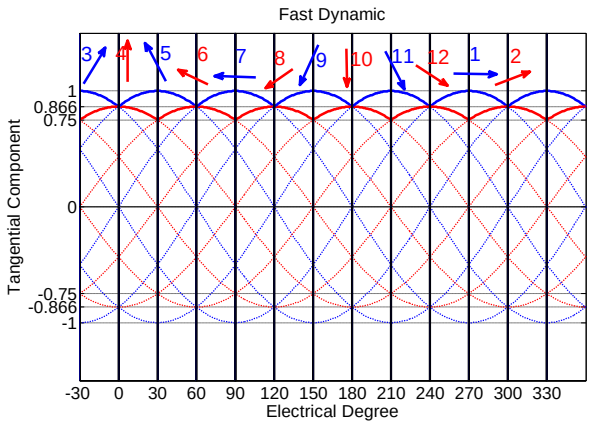

Fig.5. tangential components in rapid torque scheme

Simulation Results

Fig.6 illustrates the torque and flux responses of a permanent magnet synchronous motor under the conventional DTC with six voltage vectors and proposed DTC with twelve voltage vectors. In the proposed method vectors energy spend to increase torque rather than flux so its torque response is much faster. On the contrary, In the conventional method flux has a faster response compared to proposed method. in the proposed method unlike the conventional method flux reaches to its reference value after torque settled in the band.

For this motor, torque developing time reduced from 2.286ms to 1.807ms which is 26% improvement when the torque reference is set to half of its nominal value.

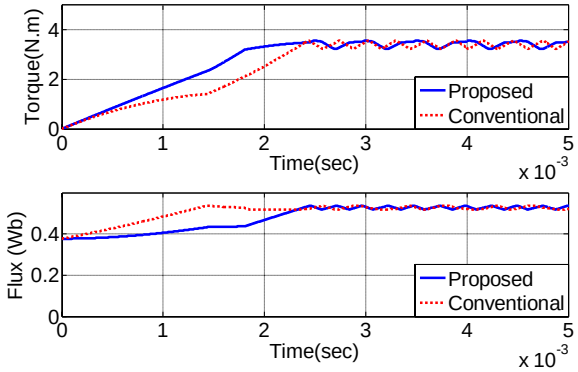

Fig.6. Torque and flux response in the conventional and proposed DTC

Fig. 7, 8 show the flux vector trajectory for the conventional and proposed DTC. In the proposed method, those vectors are chosen which have bigger tangential component compared to radial component so cause flux rotation rather than flux amplitude changes. Thus the flux trajectory goes straight ahead up in Fig. 8 to increase its angle rapidly. Adjusting the flux amplitude to the reference value is on the second priority for this control method. On the contrary, flux trajectory in the conventional DTC in Fig. 7 has a approximately 45 degree movement at the beginning to provide both flux angle and amplitude to their reference value with the same priority.

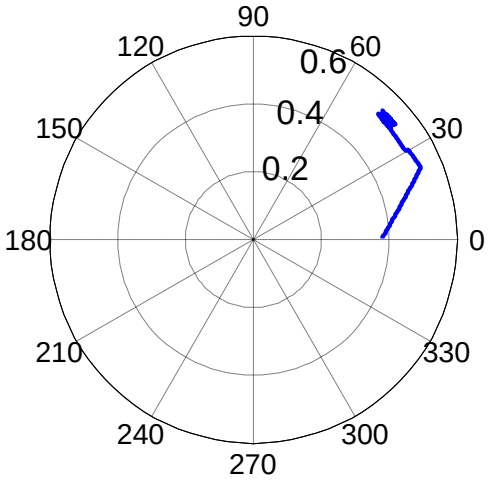

Fig.7. flux vector trajectory, conventional method

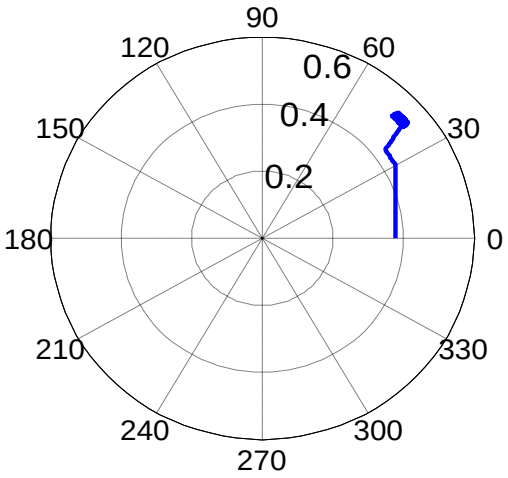

Fig.8. flux vector trajectory, proposed method

Conclusion

This paper has presented a combined switching method to improve torque dynamic performance of permanent magnet synchronous motor DTC drive. For the cited motor, torque development period reduced to 74% for half of nominal torque value and to 82% for nominal torque value.

This achievement is done via changing the look up table to include other six voltage vectors and proper selecting of them. So the simplicity of DTC structure does not disturbed and parameter independency of original DTC is sustained.

Appendix

Motor specifications:
Rated speed = 1800 rpm
λ_m = 0.314 Wb, L_d = 42.44 mH, L_q = 79.57 mH
P =2 (no. of pole pairs), Rated Torque = 3.96 Nm
J = 0.003 Nm sec2/rad (Inertia)
R_s = 1.93 Ω, R_c =460 Ω
Rated Current = 3 A
B = 0.0008 Nm/rad/sec (Viscous friction)
Inverter DC Voltage = 240 V.

References

[1] P. Vas, “Sensorless Vector and Direct Torque Control,” Oxford University press, 1998.

[2] H. Ghasemi, S. Vaez-Zadeh, “A very fast direct torque control for interior permanent magnet synchronous motors start up, ” *Energy Conversion and Management,”* **volume 46**, pp. 715-726, (2005).

A Low Torque Ripple DTC Approach by Employing Twelve Voltage Vectors

Mehdy Khayamy, Sadegh Vaez-Zadeh
School of Electrical and Computer Engineering, University of Tehran , Iran
Email: m.khayamy@ece.ut.ac.ir, vaezs@ut.ac.ir

Abstract: *A drawback of Direct Torque Control (DTC) in ac electric motors is known to be high torque ripples. In this paper a combined switching pattern is proposed to reduce torque ripples in steady state conditions. This obtained by applying appropriate voltage vectors from a set of 12 available vectors. Extensive simulation results confirm the theoretical analysis.*

Keywords DTC, Torque Ripple, Voltage Vector, Switching pattern, Drive

Introduction

Direct torque control (DTC) of induction and synchronous motor has gained popularity in the industry and researches mainly due to its simplicity and lower parameter sensitivity and faster dynamic response. Although the basic DTC invented in 1986 [1], various improvement has been made to the original control structure to reduce its defects and make it more practical and efficient. Torque ripple was always one of the main drawbacks of DTC technique and many suggestions proposed to reduce it during recent years.

Since this problem is mainly due to hysteresis controllers, some researches are based on torque hysteresis band modification. For example, dividing torque hysteresis into several parts which also demands more sampling frequency [2]. In some researches on-line adjustable torque hysteresis is proposed. Band width continuously changes according to machine variables and parameters to reduce the torque ripple [3]. Calculating exact needed time for applying voltage vectors is proposed as an alternative way to overcome the high torque ripple of DTC [4]. This method is sensitive to machine parameters too.

A suitable idea is to use zero voltages to slow down torque response increment or decrement slope [5], [6]. In this method, when the torque is at the desired value control system does not need to push it up or pull it down by applying a non-zero vector. Nevertheless, this method could not be applied to permanent magnet motors. There are other methods to reduce the torque ripple which require fundamental changes in the DTC structure like replacing hysteresis controllers with PI controllers [7], [8]. Proper performance of this method is completely subject to controller fine tuning.

To overcome with the above-mentioned issues, combined switching techniques for synchronous motor drives with DTC have been proposed. The proposed method is not sensitive to machine parameters, do not impose any increase in sampling frequency and do not add an SVM modulator. Nevertheless, this switching method reduces torque ripple significantly.

Voltage Vectors

Considering a conventional three phase inverter, according to state of two switches on the same column, each motor coils will connect to positive or negative side of DC Link or even becomes float. It is possible to model two switches with a 3 states equivalent switch as described in Fig.1. Therefore a conventional inverter theoretically has 64 switching states which 37 states could not be applied to inverter due to DC link shorting. The other 27 states are shown in table 1, however only 12 nonzero voltage vectors can be provided by the inverter due to practical considerations.

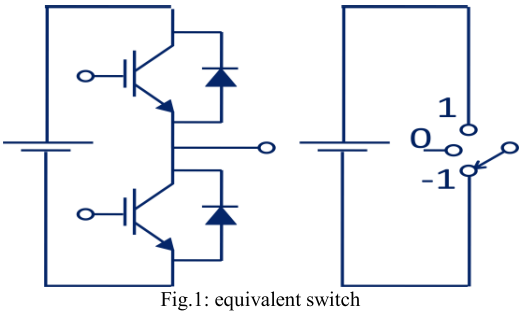

Fig.1: equivalent switch

Table (1): all possible conditions of equivalent switches

S_A	1								
S_B	1			0			-1		
S_C	1	0	-1	1	0	-1	1	0	-1
angle	Z	U2	60	U2	U1	30	300	330	0
S_A	0								
S_B	1			0			-1		
S_C	1	0	-1	1	0	-1	1	0	-1
angle	U2	U1	90	U1	Z	U1	270	U1	U2
S_A	-1								
S_B	1			0			-1		
S_C	1	0	-1	1	0	-1	1	0	-1
angle	180	150	120	210	U1	U2	240	U2	Z

In table 1 S_A, S_B and S_C are equivalent switches of phase A,B and C respectively. Angle of equivalent voltage vectors are provided in table1. Some inverter states are useless or not apply able to synchronous motor. These states are shown with Z and U1, U2 respectively.

Apply able vectors to the synchronous machine could be divided into two groups of six according to their amplitude. The vectors of each group have the same amplitude and 60º phase displacement. The vectors of the first group are displaced by 30º from those of the second group. The first

group which for each of its vector one power switch in each three inverter column must be conducting, used to applies to induction and synchronous motors DTC drive and the second group which simultaneously uses only two column to generate a vector, used to drive a BLDC motor.

Ratio of the two group amplitude is: $|\overline{U_{s1}}|/|\overline{U_{s2}}| = 2/\sqrt{3} = 1.154$. Combining these two groups could leads to better performance. In this paper wise selection of these vectors are made to slow down the torque variations inside the hysteresis band, thus providing this opportunity of choosing smaller band.

Tangential Component of Voltage and Torque

Eq. 1 shows the torque short time variation as a function of δ and angle between stator and rotor fluxes.

$$T_e = \frac{1.5P}{L_s}|\lambda_s|\lambda_m sin\delta \quad (1)$$

$$\frac{dT_e}{dt} = \frac{1.5P}{L_s}|\lambda_s|\lambda_m cos\delta\frac{d\delta}{dt} + \frac{1.5P}{L_s}\lambda_m sin\delta\frac{d|\lambda_s|}{dt} \quad (2)$$

Since flux amplitude do not change so fast comparing to flux angle, it could be supposed that $\frac{dT_e}{dt} \propto \frac{d\delta}{dt}$. It is a primary equation of DTC method. Fig. 2 represents the flux vector variation in a short time. λ_{s0} is the initial stator flux and λ_s is the stator flux after applying vector V for t seconds. knowing that $d\delta$ is a very small angle, (it is drawn with exaggeration) $d\delta$ is proportional to its sinus.

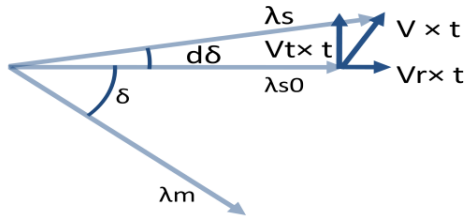

Figure (2): phasor diagram of flux and voltage vectors

Eq. 3 represents that torque short time variation is proportional to tangential component of voltage vector and inverse proportional to flux amplitude.

$$sind\delta \approx d\delta \Rightarrow \frac{V_t \times t}{\lambda_s} \approx d\delta \approx dT_e \quad (3)$$

It means that flux amplitude amount is such a undesired inertia and slows flux vector rotation. On the contrary, tangential component of voltage vector is a rotation cause.

Because of increasing voltage vector amplitude has a hardware limitation, it is good idea to concentrate on its angle to increase or decrease its tangential component and torque dynamics.

Choosing Voltage Vectors For Low Ripple Torque

Utilization of conventional DTC with six voltage vectors force us to use just one unique voltage vector in each flux zone. Other voltage vectors satisfy neither criteria of flux and torque.

Employing twelve vectors leads to the ability of choosing the applied voltage from three alternative vectors for each pair of flux and torque each having different effect on flux and torque as illustrated in Fig. 4.

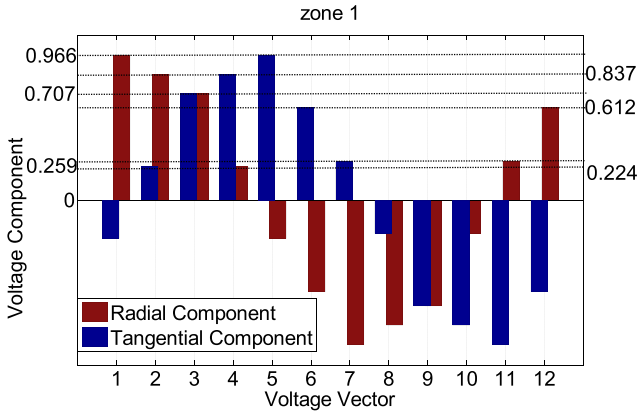

Figure (4): average voltages components when flux vector was located in the zone 1

Torque ripple has a direct relation to torque hysteresis band and bandwidth could not be reduced from a certain value which dependent on hardware limitations. For a proper DTC system, for each torque increment from lower to upper band, 8-10 samples must be taken ensuring that torque will remains in the band. In the steady state condition, if torque with lower rate increase or decrease in the band, there will be occasion to take more sample which is not really necessary and instead bring the opportunity to reduce the bandwidth as described in Fig. 5.

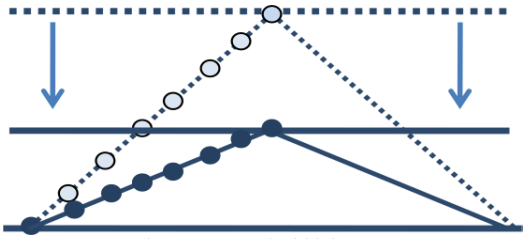

Figure (5): Band width improvement

Extending six vector and zone to twelve, two approach could be selected:

- Usual torque and usual flux response (Φ↕ T↕)
- Slow torque and rapid flux response (Φ↑ T↓)

Although the first approach is using twelve vector, it approximately has the same response as using conventional six vector. It uses vectors 3,6,9,12 for zone1 (0-30º). Voltage vector energy in the second approach have a reduced effect on torque changes. Considering Fig. 4 for zone1, vectors 2,6,8,12 could be selected for this approach. They have minor effect on torque increment or decrement. Therefore, a lower hysteresis band can be chosen which results in lower torque ripples. Table2 illustrates zone1 (one part of look up table) for transient and steady state conditions. In the steady state condition torque priority must be low and approach two will be selected.

Due to symmetry, vector numbers for zone two could be obtained by adding one two each number of table2. With the similar way, vector numbers of all zones could be achieved by

adding the number of corresponding vector in zone 1 with the subtraction of that zone number from one.

Table (2): zone 1 ,one part of lookup table

Zone1	Decrease Torque		Increase Torque	
Decrease Flux	Torque	V	Torque	V
	↓	8	↓	7
	↕	9	↕	6
Increase Flux	Torque	V	Torque	V
	↓	1	↓	2
	↕	12	↕	3

Simulation Results

Fig. 6 illustrates the torque responses of a permanent magnet synchronous motor under the conventional DTC with six voltage vectors and proposed DTC with twelve voltage vectors. Using twelve voltages leads to slower response with low slope of torque change. This provides the opportunity of decreasing the hysteresis band in steady state and fixed sampling time. The details of choosing correct vectors will be presented in the full paper.

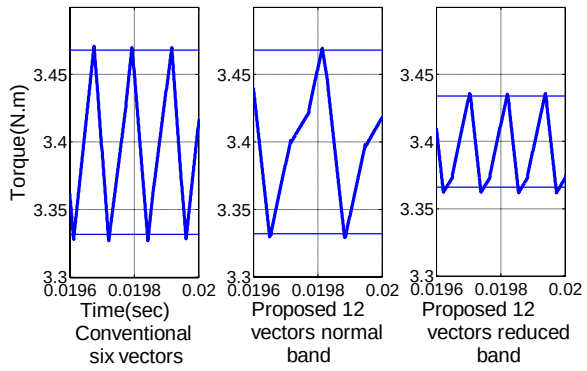

Figure (6): Comparing torque response of conventional and proposed method

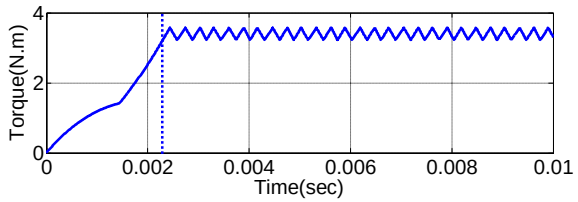

(a)

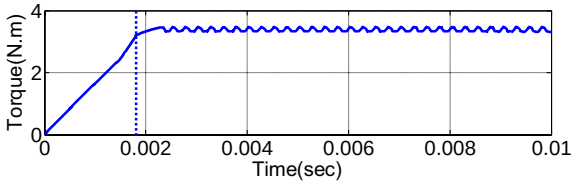

(b)

Figure (7): Comparing torque response of (a) conventional and (b) proposed method

Conclusion

The combined switching method presented in this paper has proved to be capable of reducing torque ripple significantly. Parameters of applied motor are presented in the appendix. For this motor, torque ripple reduced to 40% compared to conventional DTC. This method is independence of motor parameters variation and it done in the stationary coordination system, so do not impose extensive calculation to the control method like park transformation.

Appendix

Motor specifications:
Rated speed = 1800 rpm

λ_m = 0.314 Wb, L_d = 42.44 mH, L_q = 79.57 mH

P =2 (no. of pole pairs), Rated Torque = 3.96 Nm

J = 0.003 Nm sec2/rad (Inertia)

R_s = 1.93 Ω, R_c =460 Ω

Rated Current = 3 A
B = 0.0008 Nm/rad/sec (Viscous friction)
Inverter DC Voltage = 240 V.

References

[1] I. Takahashi and T. Noguchi, “A new quick-response and high-efficiency control strategy of an induction motor,” *IEEE Trans. Ind. Appl.*, vol. IA-22, no. 5, pp. 820–827, Oct. 1986.
[2]J. Koo Kang, S. Ki Sul “New direct torque control of induction motor for minimum torque ripple and constant switching frequency,” IEEE Trans. on Industry Applications, Vol. 35, No. 5, Sep/Oct 1999.
[3]S. Vaez-Zadeh G.H. Mazarei “Open loop control of hysteresis band amplitudes in direct torque control of induction machines,” in Proc. IEEE Conf., Industry Applications Conference, Vol. 3, pp. 1519-1524, 2000.
[4] V. Ambrozi, G. Buja and R. Menis “Band-constrained technique for direct torque control of induction motor,” IEEE Trans. on Industrial Electronics, Vol. 51, No. 4, Aug. 2004.
[5] D. Telford, M.W. Dunnigan, and B.W. Williams “Novel torque-ripple reduction strategy for direct torque control,” IEEE Trans. on Industrial Electronics, Vol. 48, No. 4, Aug. 2001.
[6] Y. Lai, W. Wang and Y. Chen “Novel switching techniques for reducing the speed ripple of AC drives with direct torque control,” IEEE Trans. on Industrial Electronics, Vol. 51, No. 4, Aug. 2004.
[7] L. Tang, L. Zhong, M. Fazlur Rahman and Y. Hu “A novel direct torque control for interior permanent-magnet synchronous machine drive with low ripple in torque and flux—a speed-sensorless approach,” IEEE Trans. on Industry Applications, Vol. 39, No. 6, Nov./Dec. 2003.
[8] L. Tang, L. Zhong, M. Fazlur Rahman and Y. Hu “A novel direct torque controlled interior permanent magnet synchronous machine drive with low ripple in flux and torque and fixed switching frequency,” IEEE Trans. on Power Electronics, Vol. 19, No. 2, Mar. 2004.
[9] P. Vas, “Sensorless Vector and Direct Torque Control,” Oxford University press, 1998.

Semiconductor Aided On – Load Voltage Regulation of Power Transformers

Tony Dragomirov and Nikolay R. Gourov

Abstract: *The paper is presenting systemization of schemes for switching operations performed by semi-conductor switching elements such as diodes, thyristors and others. The comparison of electrical loading between different switching schemes and recommendation for each particular scheme are given as well.*

On base of the above study conclusions, the Hyundai Heavy Industries Co., Bulgaria is currently developing the On-Load Tap-Changer (*OLTC) with diverter switch based on thyristor type switching elements.*

Keywords*: On-Load Tap-Changer, Voltage Regulation, Power Transformer, Semiconductor, Diverter Switch.*

Introduction

Factory in Sofia where OLTCs are produced has now fifty years tradition of producing these high-tech. sophisticated products. Up to 1990 Bulgaria used to be one of the biggest producers of OLTCs of the world. After that, as a result of improvident economic policy of the state supervened collapse of the whole industry as well as of this production. In 1997 the factory became property of Hyundai Heavy Industries, republic of Korea and since then starts the revival of development and production of OLTCs. Production was modernized and the broad range of existing sets of OLTCs was significantly improved. New constructions on the base of use of vacuum interrupters (VI) were developed. To hold on its position in the competition with other leading factories in the world Hyundai Heavy Industries – Sofia is investigating and developing other tendencies as well. One of them is to use as commutating elements different power semiconductors.

The voltage regulation of power transformers under load by means of built-in On-Load Tap-Changers is still the most used method by transformer manufacturers and power electricity network authorities. The application of semiconductor elements in the OLTCs' diverter switch as power switching elements is well known method since many years but not widely used till now due to capacity and reliability of those semiconductor elements. As a result of improved design, technology and quality of semiconductor elements from one hand and increased requirements regarding electrical wearing quality of power switching elements on the other hand. There is increased interest for their implementation in OLTCs.

Basic schemes of semiconductor aided diverter switches

The existence of numerous schemes of switching over of OLTCs' diverter switches is known [1]. Contact systems of diverter switches of classical type extinguish arcs in transformer oil. The oil is contaminating and the working conditions are worsening. When the running currents are high enough the arc extinguishing during the second or even during the third passing of the alternating current through the null value. This is dangerous because exists possibility of step short circuit and failure. German manufacturer "Transformatoren Union AG" is proposed different schemes [2], in which power diodes are mounted in series or in parallel to the classical contacts. Example of this is shown on Fig. 1. Here is used the most widespread switching scheme named "flag" [1]. The diverter switch is connected to the taps N_1 and N_2 of adjusting coil L of the transformer. Here K_1 are main contacts, K_2 – auxiliary contacts, K_0 – parallel, permanently conducting the current contacts, R – current limiting resistors and N_0 – terminal. Every of contacts K_1 and K_2 is divided to two parallel branches with diodes connected in series. Arc is appearing on this branch through which the diode lets the current to pass. After the current passes through null value contact elements are moved away and second arc is not appearing. Thus switching ability rises and electrical wearing lowers. Because of complicated construction and augmented dimensions of the diverter switch these schemes have had restricted application.

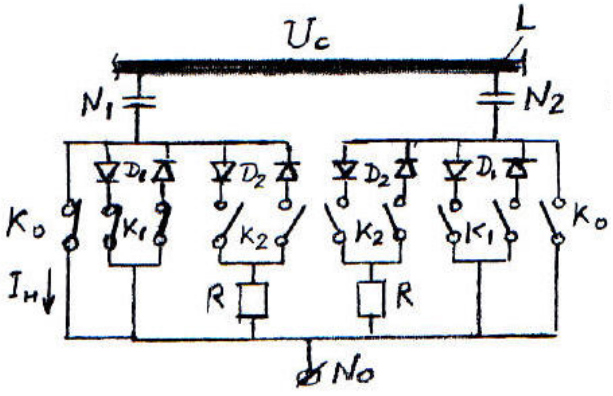

Fig. 1 Scheme with diodes mounted together with the classical contacts

The scheme of Fig. 2 [3] is interesting. Thyristor T in parallel to a synchronized contact CK is used. First K_0 is opened without arc, after that K_1 is switched; CK is opening during the half-cycle, when T is conducting and K_2 is switched during the next period. If use two synchronized contacts CK_1 and CK_2 (Fig. 3) it is possible to realize the switching with use of only one diode D. In these schemes as well as in all presented further control

schemes will not be discussed, because this will be done in other work. In the former "Electrical Power Technique Institute" (EPTI) – Sofia has been experimented switching process with synchronized contacts. Partial erosion was found out. The conclusion is that application of these schemes is not practical because of complication of kinematics and control.

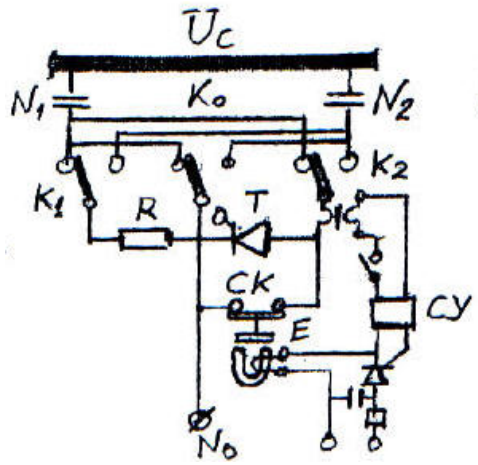

Fig. 2 Scheme with thyristor

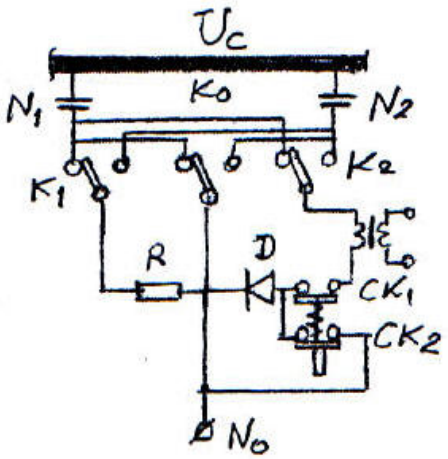

Fig. *3 Scheme with two synchronized contacts*

Scheme of switching of thyristor aided diverter switch produced by the Austrian manufacturer "Elin" (now in the structure of "Mashinenfabrik Reinhauzen GmbH) is given on Fig. 4 [4]. It works as follows: with the thyristor group T switched-off, K_2 is shifting and K_1 is closing; T is switching-on and K_0 is opening; T is switching-off and K_3 is shifting; T is switching-on, the other K_0 is closing and T is switching-off again and K_1 is opening. Disadvantages here are: complicated contact system and control; T is commutating sum of nominal and circulating currents; there is erosion of K_1 due to arcs during switching-on process.

Diverter switches shown on Fig. 5 and Fig. 6 [6] didn't contaminate the oil. Here, there is combination of thyristor group T and VI (V_1 and V_2). With T switched-off K_1 is shifting; V_1 is switching-off and during the first passing of alternating current through the null value for short period of time small current is flowing through the control system CY and control contact KY, as result of this T is switching-on (Fig. 5). On Fig. 6 there are two VI, this leads to simplification of the kinematics and increasing of electrical wearing quality.

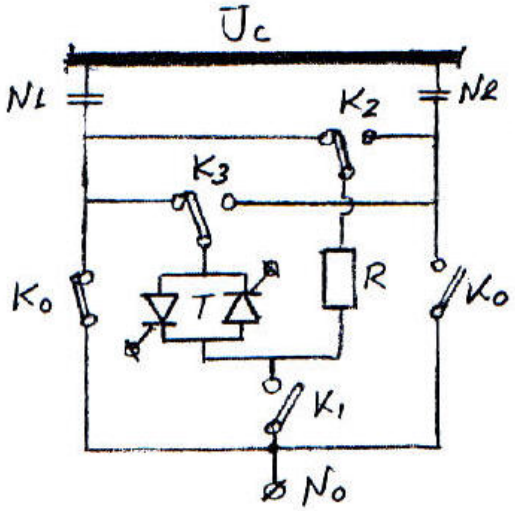

Fig. 4 Scheme of thyristor aided diverter switch

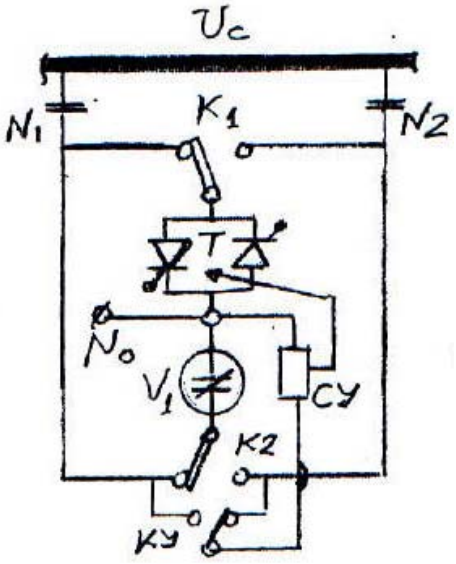

Fig 5 Scheme with both thyristor group and vacuum interrupter

Scheme for arc-free switching with two thyristor groups T_1 and T_2 is shown on Fig. 7 [6]. It works without resistor. Shifting of the current from T_1 to T_2 is occurring during small period of time (t_0) when the alternating current is passing through the null value. With starting of switching process and T_2 in blocking mode K_2 is shifting, after that KY is closing and control system CY is passing control current to T_1. It is starting to conduct and permanently conducting the current contact K_0 is opening arc-free. Following is KY opening and T_1 is switching to blocking mode during the first passing of the current through the null value. For short period of time ($t_0 \approx 100$ μs) small current is passing through CY and it elaborates gate triggering current for T_2. After that K_0 is

connecting to N_2 and K_1 is shifting. Kinematics here should be such that switching in both directions to be realized from T_1 to T_2. If there is need to switch from T_2 to T_1 CУ should be doubled which complicates the device. During the eighties of the last century in the Institute of Electrical Engineering together with Electrical Apparatus Department of Technical University – Sofia was made experimental specimen according to the scheme on Fig. 7. Later the work was not continued, because at that time had lack of reliable quality thyristors.

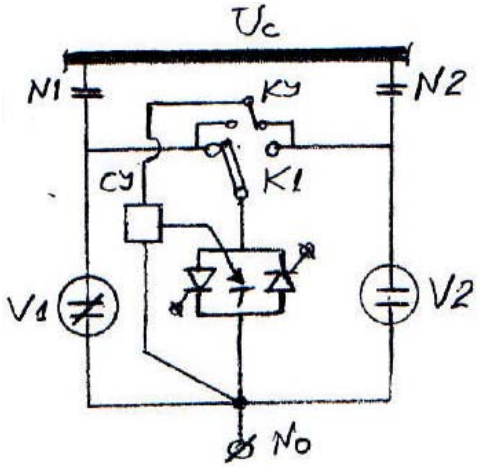

Fig. 6 Combined scheme with thyristor group and two vacuum interrupters

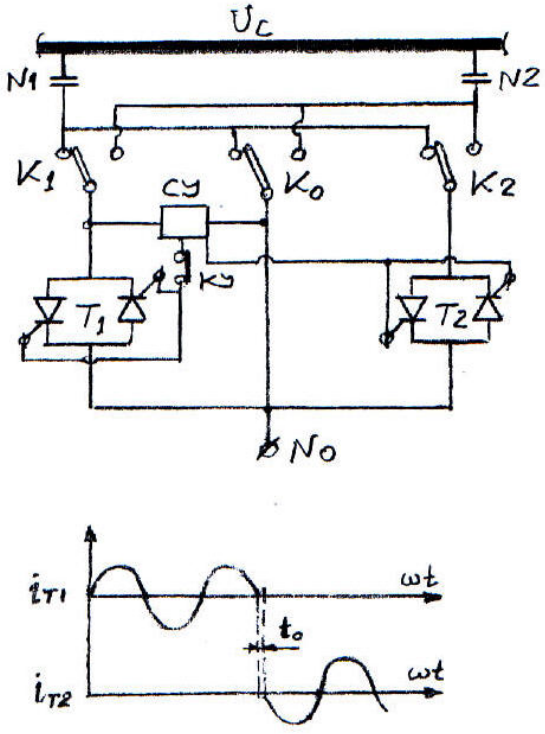

Fig. 7 Scheme for arc-free switching with two thyristor groups

Now in Hyundai Heavy Industries – Bulgaria thyristor aided diverter switch is developing according to the scheme shown on Fig. 8. The resistor R is used for increasing of safety. Sequence of switching of particular commutating elements is shown on the same figure. Here dark sectors correspond to switched-on element. Kinematics is such that in both directions of switching the current is passing from T_1 to T_2. Thus the currents and the recuperating voltages of T_1 and T_2 are significantly lower than in the case of symmetrical work.

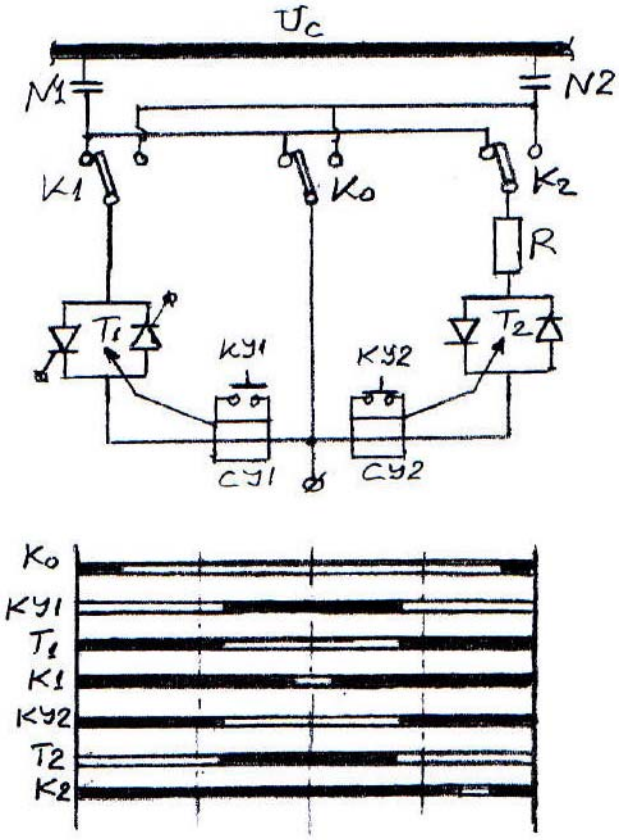

Fig. 8 Scheme of the thyristor aided diverter switch chosen from Hyundai Heavy Industries Co., Bulgaria

The difference between both switching methods will be cleared by the following practical example: Diverter switch for nominal current I_H=1600 A and step voltage U_C=2500 V is developing. According to the international standard IEC 60214 – 1, 2003 the switching ability is proved by testing with $2.I_H$=3200 A. The value of resistor is chosen to be R=1 Ω. In scheme with obligatory switching from T_1 to T_2, the thyristors from group T_1 are opening with current 3200 A and recuperating voltage is $2.I_H$=2.1600.1=3200 V. Group T_2 is loaded with the circulating current $I_C=U_C/R$=2500 A and recuperating voltage U_C=2500 V. Thyristors with I_H=2000 A and U_H=5000 V are used. They can carry-off up to 10000 A impulse current. Reserve is foreseen, because the diverter switch is working in hot transformer oil.

In symmetrical scheme of switching the current of T_1 will be $2.I_H+I_C$=5700 A and recuperating voltage $2.I_H.R+U_C$=5700 V. Therefore in this case the nominal parameters should be about twice lower.

For comparison in the scheme from Fig. 7 T_1 and T_2 are loaded with 3200 A and 2500 V, which doesn't

giving considerable advantages, however exists uncertainty because of absence of resistor.

Conclusion

Analysis of presented switching schemes shows that the most suitable for practical use is this from Fig. 8. It is chosen from Hyundai Heavy Industries Co., Bulgaria for development of diverter switch.

References

[1]. Драгомиров Т, И. Ячев Електрически апарати за високо напрежение, ИК "ICON", 1994;

[2]. Patent № 2611570 – Germany;

[3]. Авторско свидетелство № 13830 – Bulgaria;

[4]. Elin OLTC Hybrid – Diverter Switch with Thyristors type TADS;

[5]. Авторско свидетелство № 27501 – Bulgaria;

[6]. Авторско свидетелство № 14469 – Bulgaria.

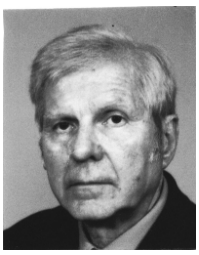

Tony Dragomirov was born in Pernik, Bulgaria on May 6, 1934. He has graduated from the Technical University – Sofia as M.Eng. in Mechanical Engineering in 1959 and received second M.Eng. degree in Electrical Engineering from the same university in 1965. In 1969 he received his Ph.D. degree and in 1990 D.Sc. degree.

Dr. Dragomirov has the rank of Senior Research Fellow from the Institute of Electrical Engineering – Sofia since 1986 and Professor from the Technical University – Sofia since 1992.

Tony Dragomirov is HV Apparatuses Technical Director of Hyundai Heavy Industries Co., Bulgaria, 41 Rojen Blvd., 1271 Sofia, Bulgaria (e-mail: tdragomirov@hhi-co.bg).

Nikolay R. Gourov was born in Sofia, Bulgaria, on August 31, 1963. He studied at the Technical University – Sofia, Bulgaria and graduated as M.Eng. in Electrical Engineering in 1988.

Since 1996 he works in the Department of Electrical Measurements from Faculty of Automatics of the Technical University – Sofia as an assistant professor. His scientific interests include Non-Destructive Testing, Measurement of Non-Electrical Quantities, Intelligent Measurement Systems, Partial Discharges and On-Load Tap-Changers with Special Elements.

Nikolay R. Gourov is with the Department of Electrical Measurements, Faculty of Automatics, Technical University – Sofia, 8 Kl. Ohridski Blvd., 1000 Sofia, Bulgaria (e-mail: nrg@tu-sofia.bg).

On-Load Tap-Changers with Vacuum Interrupters for On-Load Regulation of Power Transformers

Tony Dragomirov and Nikolay R. Gourov

Abstract: *The present study is presenting systematization of utilized design variants by leading manufacturers of On-Load Tap-Changers* (*OLTC*) *regarding the application of diverter switches with Vacuum Interrupters* (VI). *On the base of performed comparison and analyses, the main technical tendencies are underlined as well as their application in the developed new OLTC series with VI manufactured by Hyundai Heavy Industries Co., Bulgaria.*

Keywords: *On-Line Tap-Changer, Power Transformer, Vacuum Interrupter, Voltage Regulation.*

Introduction

The leading manufacturers of (OLTC) - Mashinenfabrik Reinhausen (MR)-Germany, ABB-Sweden and Hyundai Heavy Industries (HHI)-Bulgaria have implemented Vacuum Interrupters in their new types OLTCs developed and in regular production during last years. The implementation of VI as power switching element is providing important operational and maintenance advantages.

It is known [1], that the most widespread voltage regulation method in power engineering and industry is by use of OLTC incorporated into the power transformers. On-Load Tap-Changers are among the most sophisticated and expensive high voltage apparatuses. Depending on the parameters set of OLTC, motor unit and accessories are sold from € 15 000 to € 100 000. One of the leading manufacturers of these products worldwide, according to growth and production is the plant of Hyundai Heavy Industries (HHI) in Sofia. This is a plant with 50 – years of tradition in the field of OLTC. Competition in worldwide scale is very heavy mainly in the person of the biggest manufacturer in the world Mashinenfabrik Rainhauzen (MR) – Germany. In the last years competition is in the area of development of modern OLTC with vacuum interrupters (VI). In the paper analyses and comparisons will be done to characterize this development.

Main types OLTCs with VI

Advantages of the OLTCs with utilization of VI in comparison to the classical types with arc-damping in oil are significant. The oil in the oil-compartment of the OLTC has not being contaminated, which leads to reduction of maintenance, to rise of electrical wearing quality and prolongs the revision periods several times. The commutation reliability is rising. There is no necessity of filtration devices for oil purification.

The trend of development of new series of OLTCs with VI is to change only the power switch, but oil-compartment, change-over selector and fine tap selector remain the same as before. This is making easier to a considerable degree production of OLTCs and their application to construction and exploitation of transformers.

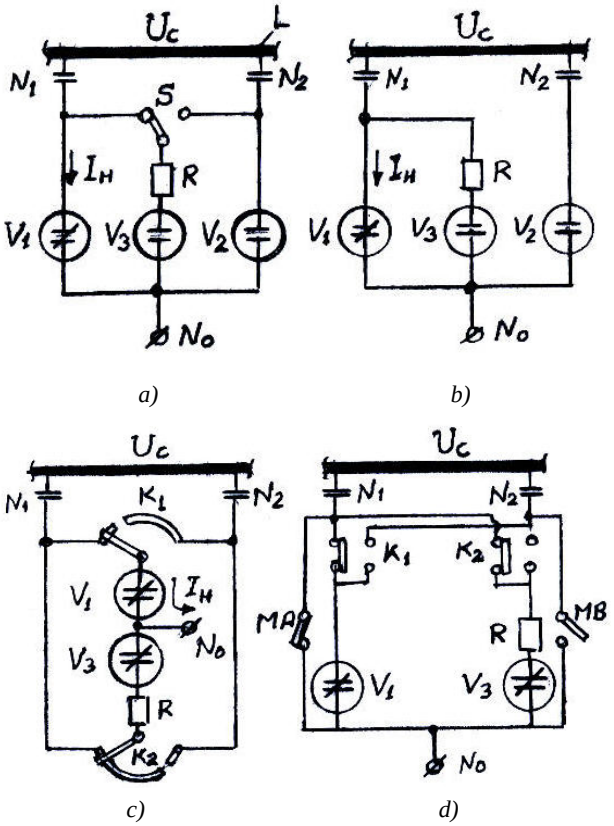

Fig. 1 Practical switching schemes with VIs

As a matter of principle, every switching scheme [1] can be transformed to one with utilization of VIs. This can be done by replacement of every contact junction which is damping arcs in oil with VI. Such variant is not always economically advantageous. Thus limited number of schemes is suitable for practical application. that sort of switching schemes are systematized in [2]. In this paper, however only schemes, which already has been used in real diverter switches will be treated. Four such schemes are shown on Fig. 1. For evaluation of these schemes it is important to know currents interrupted by every one of the VI and recuperating voltages between contacts, after extinguishing the arc during the first pass of the alternative current through null value. This

describe the efficiency of the given diverter switch regarding to switching ability and electrical wearing quality. These values for the schemes from Fig. 1 are systematized in Table 1.

Table 1

Currents and voltages for the schemes from Fig. 1

Scheme from Fig. 1	Switching from N1 to N2		Switching from N2 to N1	
a	$I_{V1}=I_H$ $U_{V1}=I_H.R$	$I_{V3}=U_C/R$ $U_{V3}=U_C$	$I_{V2}=I_H$ $U_{V2}=I_H.R$	$I_{V3}=U_C/R$ $U_{V3}=U_C$
b	$I_{V1}=I_H$ $U_{V1}=I_H.R$	$I_{V3}=U_C/R$ $U_{V3}=U_C$	$I_{V2}=I_H \pm U_C/R$ $U_{V2}=I_H.R \pm U_C$	$I_{V3}=0$ $U_{V3}=0$
c	$I_{V1}=I_H$ $U_{V1}=I_H.R$	$I_{V3}=U_C/R$ $U_{V3}=U_C$	$I_{V1}=I_H \pm U_C/R$ $U_{V1}=I_H.R \pm U_C$	$I_{V3}=0$ $U_{V3}=0$
d	$I_{V1}=I_H$ $U_{V1}=I_H.R$	$I_{V3}=U_C/R$ $U_{V3}=U_C$	$I_{V1}=I_H$ $U_{V1}=I_H.R$	$I_{V3}=U_C/R$ $U_{V3}=U_C$

Symbols on Fig. 1 are as follows: V_1 and V_2 – main VIs; R – resistor, V_3 – auxiliary VI; N_1 and N_2 – contacts of the change–over selector, connected to the neighboring taps of adjusting coil of the transformer L; N_0 – terminal; S – switching contact junction; K_1 and K_2 – other variant of switching contact junctions; MA and MB – parallel contact junctions.

Symbols on Table 1 are as follows: I_H – nominal current of the tap-changer; U_C – step voltage; I_{Vn} – current interrupted by the respective VI; U_{Vn} - recuperating voltage. Sign "+" or "-" is according to the regulation direction [1]. Number of switching over actions with both signs is equal.

Scheme from Fig. 1a is used in diverter switches of OLTC RSV9 of Hyundai Heavy Industries [3], which are designed for nominal currents 400 A, 550 A and 700 A. According to the same scheme is working RS21 of HHI, which is designed for transformers with SF6 –gas as insulating environment [4]. The scheme of Fig. 1b is applied in RSV5 of HHI. This is an OLTC designed for technological needs' transformers with insulated phases (one from another) and nominal voltages under 36 kV. The nominal current is 1200 A, and the step voltages are small. In this case circulating current $I_C=U_C/R$ is small and has no important effect on switching capability and electrical wearing quality. In exchange to this the construction is simplified. The scheme of Fig. 1c is used in OLTC RSV20 and RSV12 of HHI. Nominal currents are up to 400 A, because of which the asymmetry of electrical load shown in Table 1 has no significant effect. This allows constructions to be simplified. Scheme from Fig. 1d is used in the set of OLTC type VR of MR [5]. Typical for this type of diverter switches is that in both directions of switching firstly is commutating V_1 and after that V_3. This has been reached by complicating of mechanical construction. In exchange the electrical load is decreasing. Parallel contact junctions MA and MB exist in the scheme, which facilitates K_1 and K_2.

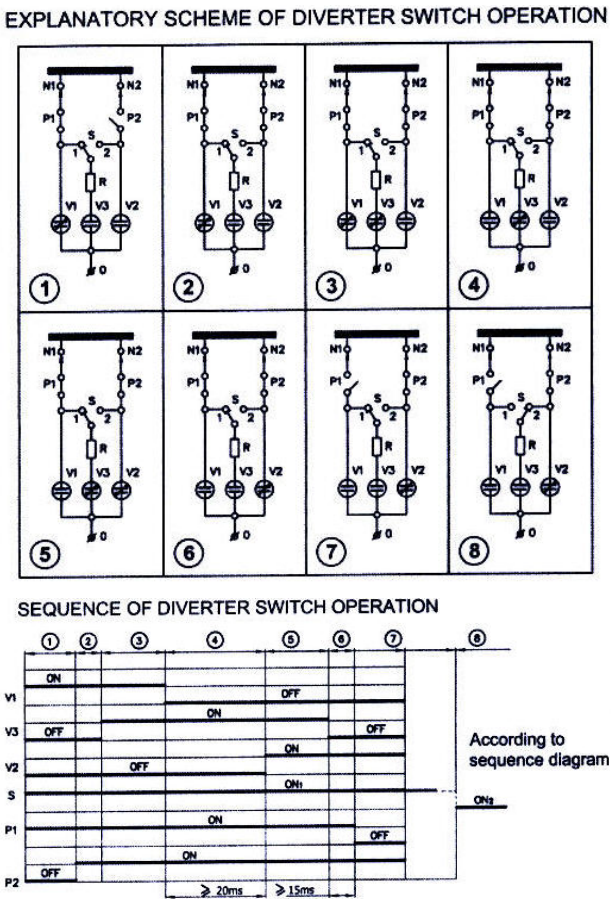

Fig. 2 RSV9 Diverter switch operation

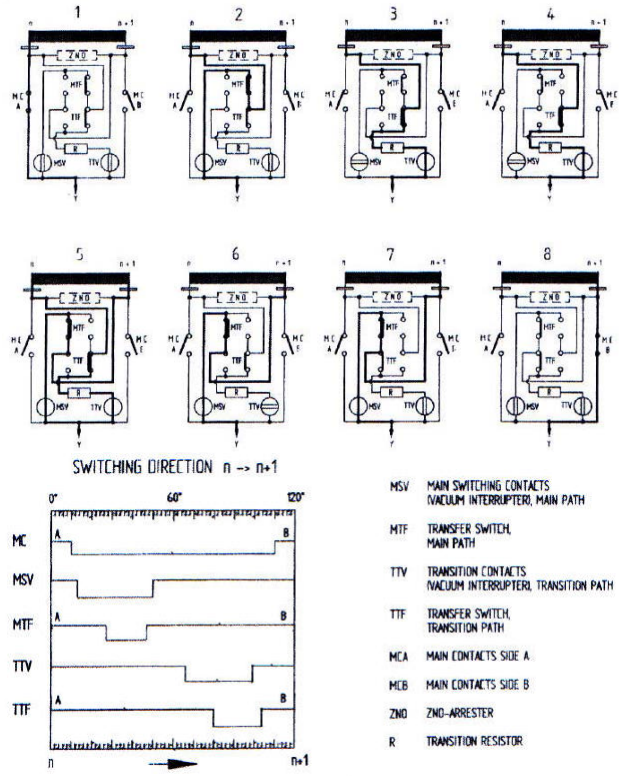

Fig 3 VCR's switching sequence from n to n+1

It is of interest to make brief comparison between OLTC RSV of HHI and VRC of MR. Sequence of switching from N_1 to N_2 of RSV9 [3] is shown on Fig 2. Compared to the Fig. 1a here have been added breaking contact junctions P_1 and P_2. They are used in case of high impulse step voltages of the respective transformer. The sequence of switching of MR's VRC is represented on Fig. 3, where house symbols are preserved [5]. This set is for nominal currents 400 A, 550 A and 700 A too.

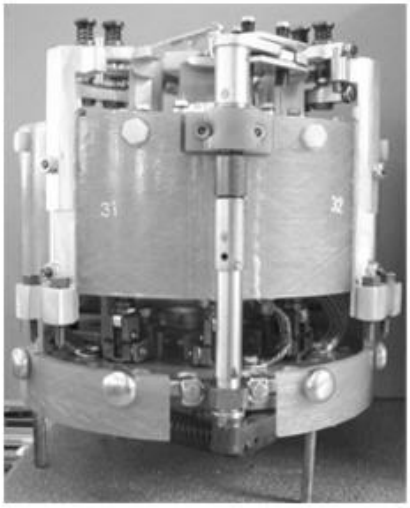

Fig. 4 RSV9 in single-phase implementation

For visual comparison on Fig. 4 is shown picture of RSV9 in single-phase implementation. On Fig. 5 RSV9 can be seen in three-phase implementation. Unification of both constructions is high. On the picture of Fig. 6 can be seen pull-out part of the diverter switch of VRC. It is built in oil compartment of VRC that is not shown on the picture. On the inner surface of this oil tank are placed immovable contact junctions.

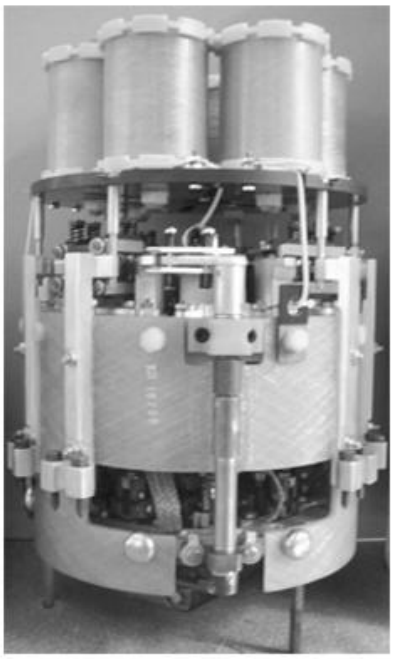

Fig. 5 RSV9 in three-phase implementation

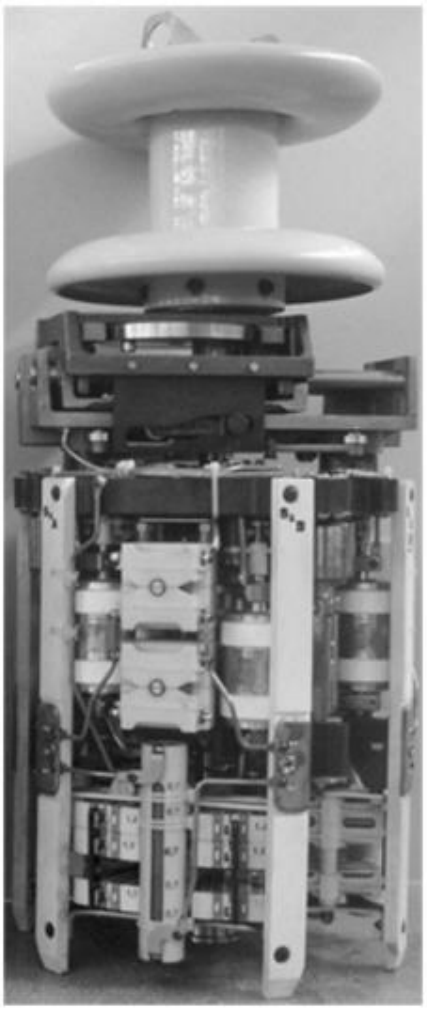

Fig. 6 Pull-out part of OLTP VRC of MR

OLTC RSV9 ensures some significant advantages such as:

- The diverter switch utilizing VI is interchangeable with the one extinguishing arcs in oil. This means that replacement can be done of operating in exploitation diverter switches. At the same time this is great advantage during the production process.
- The diverter switch can be assembled and controlled as a separate assembly, which is done out of the oil compartment.
- Using of three VIs on phase instead of two is raising the cost of production to certain degree, but this is compensated even in greater extent by the simplified construction. In exchange to this, when equal quality VIs are used, electrical wearing quality is raising up to 50 %.
- When contact junctions connected in parallel to VI are used erosion of contact surfaces is received, which require use of metal-ceramic capping. Thus partial contamination of the oil is available, but the task when VIs are used is not to have such. In RSV's diverter switches have no contact junctions connected in parallel.

Conclusion

Hyundai Heavy Industries – Bulgaria has developed some sets of OLTCs with VI. They have very high technical parameters and ensure significant production and exploitation advantages. This strengthens Hyundai Heavy Industries – Bulgaria's position as one of the leaders in development and production of OLTCs worldwide.

References

[1] Драгомиров Т, И. Ячев Електрически апарати за високо напрежение, ИК "ICON", 1994;

[2] Dragomirov T. Application of SF6 Gas in On-Load Tap-Changers, Proceedings of XI-th International Symposium on Electrical Apparatus and Technologies SIELA 1999, Vol. II, Plovdiv, Bulgaria, 1999, pp. 85 - 89;

[3] On – Load Tap – Changers, Type RSV9.3, Hyundai Heavy Industries Co., Bulgaria;

[4] Dragomirov T., B. Vasilev On-Load Tap-Changer with Vacuum Interrupter for Transformers with Insulation SF6 Gas, Proceedings of XIII-th International Symposium on Electrical Apparatus and Technologies SIELA 2003, Vol. I, Plovdiv, Bulgaria, 2003, pp 110 - 113;

[5] Vacutap VR, Mashinenfabrik Reinhausen GmbH, Germany

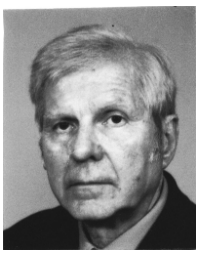

Tony Dragomirov was born in Pernik, Bulgaria on May 6, 1934. He has graduated from the Technical University – Sofia as M.Eng. in Mechanical Engineering in 1959 and received second M.Eng. degree in Electrical Engineering from the same university in 1965. In 1969 he received his Ph.D. degree and in 1990 D.Sc. degree.

Dr. Dragomirov has the rank of Senior Research Fellow from the Institute of Electrical Engineering – Sofia since 1986 and Professor from the Technical University – Sofia since 1992.

Tony Dragomirov is HV Apparatuses Technical Director of Hyundai Heavy Industries Co., Bulgaria, 41 Rojen Blvd., 1271 – Sofia, Bulgaria (e-mail: tdragomirov@hhi-co.bg).

Nikolay R. Gourov was born in Sofia, Bulgaria, on August 31, 1963. He studied at the Technical University - Sofia, Bulgaria and graduated as M.Eng. in Electrical Engineering in 1988.

Since 1996 he works in the Department of Electrical Measurements from Faculty of Automatics of the Technical University - Sofia as an assistant professor. His scientific interests include Non-Destructive Testing, Measurement of Non-Electrical Quantities, Intelligent Measurement Systems, Partial Discharges and On-Load Tap-Changers with Special Elements.

Nikolay R. Gourov is with the Department of Electrical Measurements, Faculty of Automatics, Technical University - Sofia, 8 Kl. Ohridski Blvd., 1000 Sofia, Bulgaria (e-mail: nrg@tu-sofia.bg).

Dynamic modes under speed pitch alteration of induction machine with residual magnetic field in case of load lowering

Pencho Vladimirov, Dimitar Spirov

Abstract: *A methodology, algorithms and mathematical models for determination of stator voltages, currents and linkage fluxes components and frequencies, rotor currents and linkage fluxes components and frequencies, electromagnetic moment and angular speed in case of induction machine with residual magnetic field speed pitch alteration when lowering a load have been developed.*

The model investigations present that in case of induction machine with residual magnetic field speed pitch alteration when lowering a load depending on speed alteration direction, switching time for the new speed and phase between supply voltages and electromotive force (E.M.F.) arisen from residual magnetic field, the resultant supply voltage and impact currents and moments of induction machine can be bigger than starting ones.

Keywords: *induction machine, residual magnetic field, speed pitch alteration, load lowering*

Introduction

Oftentimes the induction machines driving lifting mechanisms of cranes, hoists, elevators, etc. operate in dynamic and steady-state modes of load lowering. The literary studying present that the steady-state modes have been investigated mainly and in contrast to the dynamic ones when lowering a suspended load.

The speed pitch alteration of induction machines driving lifting mechanisms is applied in order to achieve soft starting and stopping, high productivity, precise stopping, etc. In practice occur frequently cases when switching between high and low speed and vice versa, induction machine operates at residual magnetic field.

The analytical investigation of the residual magnetic field and thus inducted E.M.F. at constant rotational speed has been done in [1,2,3]. A transient processes investigation approach for accounting of the E.M.F. and currents caused by residual magnetic field is given in [2], over again switching on and reversing of induction machine with residual magnetic field are investigated.

All-purpose mathematical model of induction machine which can be applied for all kinds of transient processes including switching off is developed in [4]. For that purpose additional resistance Rд is added to the stator phase ohmic resistance Rs. The canceling of the stator currents and electromagnetic moment is going on by giving a very large value of Rд while Rд=0 in the rest cases. The transient processes have been investigated when switching off a three-phase induction motor with cone-shaped rotor taking into account the residual magnetic field for stages: rotation of the rotor, axial rotor travel with inductances variation and case of magnetic field killing with the purpose of breaking distance decrease.

The operating and energy characteristics of induction machine regarding to dynamic and steady-state operating modes in case of suspended load lowering have been investigated in [5]. The dynamic modes in case of speed pitch alteration of induction machine with residual magnetic field when lifting a load are investigated in [6].

The aim of this paper is development of methodology, algorithms and mathematical models for determination of stator voltages, currents and linkage fluxes components and frequencies, rotor currents and linkage fluxes components and frequencies, electromagnetic moment and angular speed in case of induction machine with residual magnetic field speed pitch alteration when lowering a load. It is necessary to obtain the induction machine operating characteristics for the dynamic modes when switching from one speed to another and steady state modes also by means of models developed.

Mathematical model

A methodology, algorithms and mathematical models for determination of stator voltages, currents and linkage fluxes components and frequencies, rotor currents and linkage fluxes components and frequencies, electromagnetic moment and angular speed in case of induction machines with residual magnetic field over again switching on are developed in [6]. The mathematical models given in [6] can be used in case of load lowering also. The taking into consideration of the alteration motion direction in case of suspended load lowering can be done either by means of induction machine rotation direction change through sign change of the component $u_{s\beta}$ or by changing of moment M_c sign.

In the presence of saturation ignoring there is an exponential pattern of the rotor currents attenuation and according to the rotor current it can be written [1]:

$$i_r = I_{r1} e^{-\frac{t}{T_{R0}}}. \quad (1)$$

The rotor currents are attenuating aperiodical currents with time constant T_{R0} and their resultant magneto-motive force is motionless according the rotor.

The currents flow through the rotor winding $\mathbf{i_r}$ excite the following linkage flux in the stator winding:

$$\psi_s = L_s i_s + L_m i_r = L_m i_r = \\ = L_m I_{r1} e^{-\frac{t}{T_{R0}}} = \frac{L_m}{L_r}\Psi_{r0} e^{-\frac{t}{T_{R0}}}. \quad (2)$$

The rotor rotates with electrical angular speed ω_r according to motionless coordinate system and the full magnetic linkage flux is

$$\boldsymbol{\Psi}_\mathbf{s} = \frac{L_m}{L_r}\Psi_{r0} e^{-\frac{t}{T_{R0}}} e^{j\omega_r t} = \\ = \Psi_s \cos\omega_r t + j\Psi_s \sin\omega_r t = \Psi_{s\alpha} + j\Psi_{s\beta}, \quad (3)$$

where $T_{R0}=L_r/R_r$ is a time constant, corresponding to ideal idle running when supplying the rotor [1].

For the inducted E.M.F. components e_{s0} caused by the rotor residual magnetic field components is obtained

$$e_{s\alpha 0} = -\frac{d\psi_{s\alpha}}{dt};\ e_{s\beta 0} = -\frac{d\psi_{s\beta}}{dt}. \quad (4)$$

In order to determine the currents in the induction machine windings in case of over again switching over from one speed to another that's sufficient to use two circuits given in [2]. The first one represents the residual rotor currents i_{rd} and i_{rq}. In order that represent them in coordinate system α,β admittance that at the stage of the over again switching on the axes α,β of the motionless coordinate system coincide with the axes d,q of the rotating coordinate system respectively.

Then the currents $i_{r\alpha}$ and $i_{r\beta}$ are:

$$i_{r\alpha} = i_{rd}\cos\omega_r t - i_{rq}\sin\omega_r t; \\ i_{r\beta} = i_{rd}\sin\omega_r t + i_{rq}\cos\omega_r t. \quad (5)$$

The second circuit defines the currents obtained as a result of stator windings resultant voltages attenuation which are equal to the sums of the mains voltages and E.M.F. from the residual magnetic field without current presence in the windings

$$u_{sAp} = u_{sA} + e_{sA0}; \\ u_{sBp} = u_{sB} + e_{sB0}; \quad (6) \\ u_{sCp} = u_{sC} + e_{sC0}.$$

For the representing vectors of the resultant voltages is obtained

(7)

$$u_{s\alpha p} = \frac{2}{3}\left(u_{sAp} - \frac{1}{2}u_{sBp} - \frac{1}{2}u_{sCp}\right); \\ u_{s\beta p} = -\frac{2}{3}\left(-\frac{\sqrt{3}}{2}u_{sBp} + \frac{\sqrt{3}}{2}u_{sCp}\right) = \frac{1}{\sqrt{3}}\left(u_{sBp} - u_{sCp}\right).$$

The stator and rotor currents of the supply circuit considered are marked $\mathbf{i_s^\Sigma}$ and $\mathbf{i_r^\Sigma}$ respectively.

The electromechanical transient processes under induction machine over again switching on in case of residual magnetic field will be represented by means of model where the following currents flow through the windings

$$\mathbf{i_s} = \mathbf{i_s^\Sigma};\ \mathbf{i_r} = \mathbf{i_r^\Sigma} + \mathbf{i_{r0}}. \quad (8)$$

The currents $\mathbf{i_s^\Sigma}$ and $\mathbf{i_r^\Sigma}$ are determined as well as the process of induction machine switching on to the voltages u_{sap} and $u_{s\beta p}$ is considered and an admittance that the magnetic field is attenuated.

By $\mathbf{i_{r0}}$ is marked the current which flows through the rotor windings until the induction machine over again switching on to the mains and it is defined from the machine previous mode of operation.

The transformation of two-phase model stator currents towards three-phase induction machine ones is carried out by means of equations:

$$i_{sA} = i_{s\alpha}; \\ i_{sB} = -\frac{1}{2}i_{s\alpha} + \frac{\sqrt{3}}{2}i_{s\beta}; \quad (9) \\ i_{sC} = -\frac{1}{2}i_{s\alpha} - \frac{\sqrt{3}}{2}i_{s\beta}.$$

The software package MATHCAD has been used for solving a systems of differential equations obtained and transformed in the *Cauchy*-form [7].

Results obtained

By means of the methodology, algorithms and mathematical models developed the dynamic modes under switching on, switching over from low to high speed and vice versa of two-speed induction motor type KG II 2714-30/4 driving electric hoist with rated load capacity of *32kN*, speed of the main raising *12m/min* and speed of the micro raising *1,4m/min* in case of load lowering have been investigated. The technical data of the electric motor are given in Appendix 1. The T-shape equivalent circuit of the motor parameters determinate by a firm-producer calculating methodology accordingly different values of the slip are given in Appendix 1 also. The inertia coefficient *FI=2,0* is assumed.

The operation mode of the two-speed induction machine is as follows: switching on of the induction machine under low speed and rated load $M_c=50Nm$ and reaching to steady-state speed. A time $t_1=1,0s$ later the low-speed winding supply is switching off and voltage is applied to the high-speed winding where residual magnetic field is presented. The induction machine operates under steady-state mode at the high speed with rated load and a time *t=1,5s* later is high-speed winding supply is switching off and voltage is applied to the low-speed winding where residual magnetic field is presented. The same model is used where the induction machine parameters according to the respective rotational frequency are inserted and initial values of the quantities when switching over one speed to another are taken into account.

By means of the mathematical models the dependencies of motor developed operational characteristics in case of dynamic and steady-state modes under switching over from low to high speed have been obtained. Some of the results obtained are presented on the respective figures.

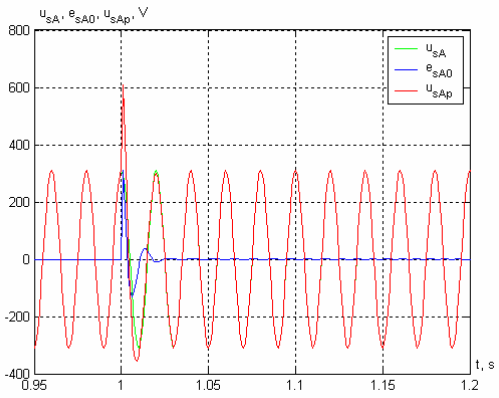

Fig. 1. Dependencies u_{sA}, e_{sA0}, u_{sAD}=f(t)

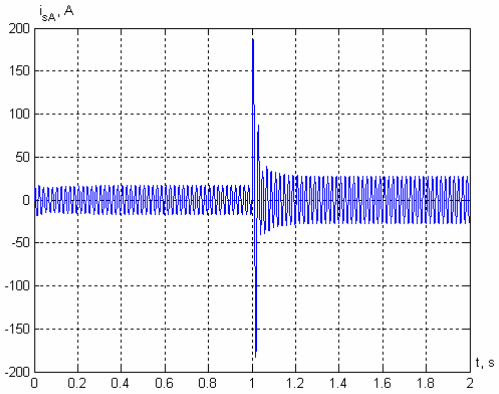

Fig. 2. Dependence i_{sA}=f(t)

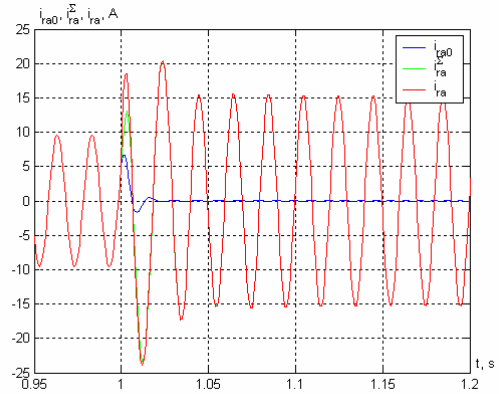

Fig. 3. Dependencies i_{rA0}, i_{rA}^{Σ}, i_{rA}=f(t)

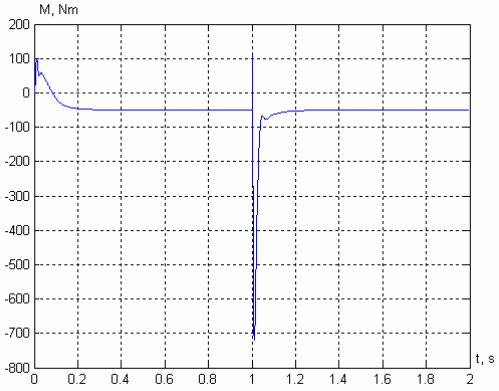

Fig. 4. Dependence M=f(t)

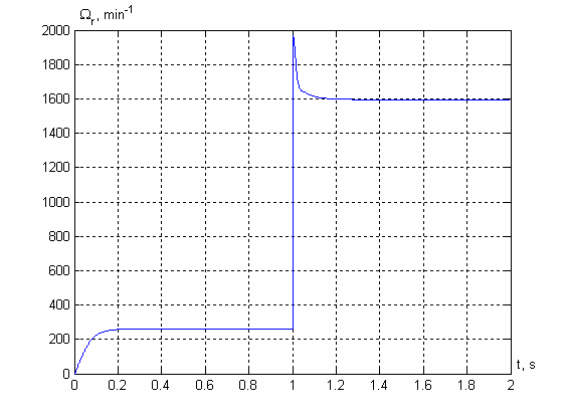

Fig. 5. Dependence Ω_r=f(t)

By means of the mathematical models the dependencies of motor developed operational characteristics in case of dynamic and steady-state modes under switching over from high to low speed are obtained. Some of the results obtained are presented on the respective figures.

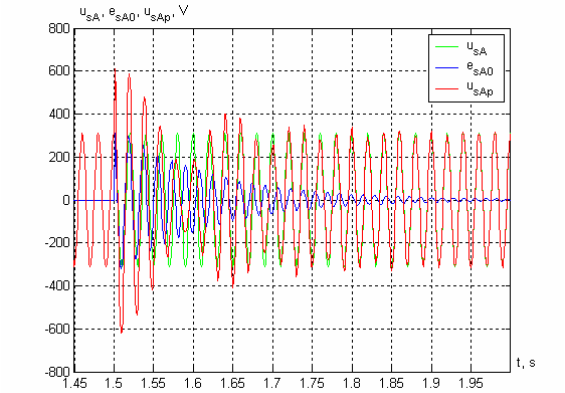

Fig. 6. Dependencies u_{sA}, e_{sA0}, u_{sAp}=f(t)

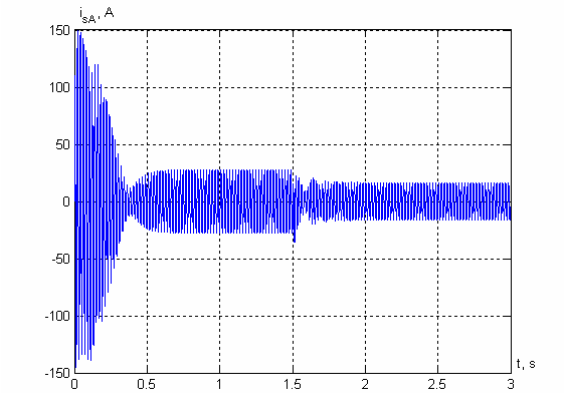

Fig. 7. Dependence i_{sA}=f(t)

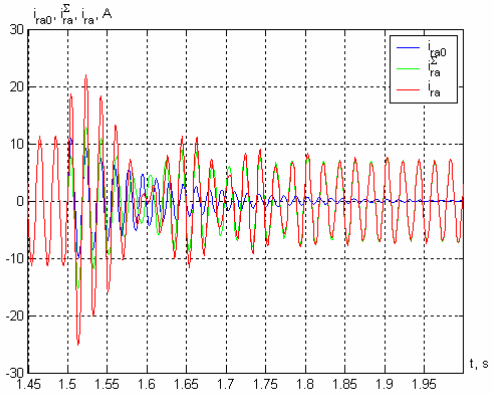

Fig. 8. Dependencies i_{rA0}, i_{rA}^{Σ}, $i_{rA}=f(t)$

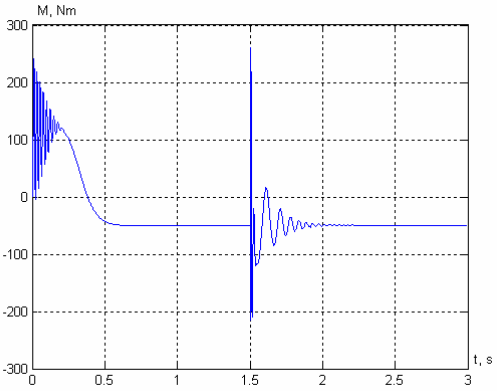

Fig. 9. Dependence $M=f(t)$

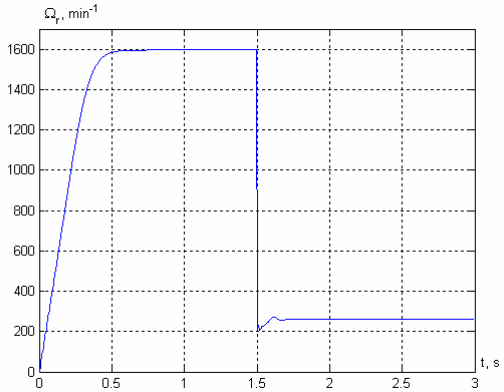

Fig. 10. Dependence $\Omega_r=f(t)$

Table 1 represents the values of U_{spmax}, i_{yd}, M_{yd} under switching on, switching over from low to high speed and vice versa.

Table 1

Table 1. Values of U_{spmax}, i_{yd}, M_{yd} under switching on, switching over from low to high speed and vice versa

	Switching on	Low-High	High-Low
U_{spmax}, *V*	311,127	617,959	607,707
i_{yd}, *A*	18,393	35,279	186,537
M_{yd}, *Nm*	99,109	163,317	691,751

From Table 1 it can be seen that under speed pitch alteration of induction machine with residual magnetic field the maximum value of the resultant supply voltage can reach value twice greater than rated one. By reason of this the impact currents and moments increase and they can be greater than starting ones.

Conclusion

The methodology, algorithms and mathematical models developed allow the determination of stator voltages, currents and linkage fluxes components and frequencies, rotor currents and linkage fluxes components and frequencies, electromagnetic moment and angular speed in case of induction machine with residual magnetic field speed pitch alteration when lowering a load have been developed.

The model investigations pointed out that in case of load lowering by induction machine with residual magnetic field speed pitch alteration the resultant supply voltage and impact currents and moments can be greater than starting ones.

Appendix 1

Technical data and parameters of the induction motor type KG II 2714-30/4

High speed

$P_N=7,5kW$; $U_N=380V$; $I_N=15A$; $f=50Hz$; $p_p=2$; $n_N=1419min^{-1}$; $s_N=0,054$; $M_N=50,47Nm$; $I_П/I_N=7$; $M_П/M_N=2,1$; $ПВ=40\%$; $ЧВ=240вкл/h$; $Jm=0,140kg.m^2$.

Parameters for slip $s=0,054$

$R_s=0,906Ω$; $X_{σs}=0,797Ω$; $R_r=0,834Ω$; $X_{σr}=0,417Ω$; $X_m=28,75Ω$.

Parameters for slip $s=1,0$

$R_s=0,906Ω$; $X_{σs}=0,795Ω$; $R_r=0,834Ω$; $X_{σr}=0,392Ω$; $X_m=27,85Ω$.

Low speed

$P_N=0,8kW$; $U_N=380V$; $I_N=13A$; $f=50Hz$; $p_p=15$; $n_N=155min^{-1}$; $s_N=0,225$; $M_N=49,29Nm$; $I_П/I_N=1,3$; $M_П/M_N=2,1$; $ПВ=10\%$; $Jm=0,140kg.m^2$.

Parameters for slip $s=0,225$

$R_s=5,327Ω$; $X_{σs}=6,63Ω$; $R_r=12,29Ω$; $X_{σr}=5,15Ω$; $X_m=14,96Ω$.

Parameters for slip $s=1,0$

$R_s=5,327Ω$; $X_{σs}=6,904Ω$; $R_r=12,30Ω$; $X_{σr}=7,09Ω$; $X_m=13,92Ω$.

References

[1] Kovacs, K. P., I. Racz. Transient processes in AC machines. Moscow, Gosenergoizdat, 1963, p. 744. (in Russian)

[2] Sokolov, M. M., L. P. Petrov, L. B. Masandilov, V. A. Ladenzon. Electromagnetic transient processes in induction machine drive. Moscow, Energia, 1967, p. 201. (in Russian)

[3] Dinov V. R., Non-symetrical modes and transient processes in electric machines. Tehnika, Sofia, 1974, p. 370. (in Bulgarian)

[4] Dinov V., E. Sokolov. Transient process under switching off the three-phase induction motor with cone-shaped rotor. Annals of Technical University - Sofia, 1974. (in Russian)

[5] Vladimirov, P., S. Rachev, D. Spirov Determination of induction machines operating and energy characteristics under dynamic and steady-state modes in case of suspended load lowering, Energetics, Sofia, №6, 2006, pp. 23-28. (in Bulgarian)

[6] Vladimirov, P., D. Spirov. Dynamic modes under speed pitch alteration of induction machine with residual magnetic field in case of load lifting. Engineering Sciences, 2008. (in Bulgarian, accepted for printing)

[7] MathCad Electronic Book – The MathSoft Electronic Book Samlper. 1994, MathSoft Inc.

Biographies

Pencho Vladimirov was born in village Gorna Lipnitza, province V.Tarnovo, Bulgaria, on December 2, 1942. He studied at the Technical University of Sofia - Bulgaria and graduated in 1968. He received the PhD degree and DSc degree, in 1978 and 2008, respectively.

Since 1970 he worked in the Technical University - Gabrovo as a lecturer. In 1982, he was elected Assoc. Prof. in Electrical Machines. His research interests include dynamic modes and loads and energy efficiency of the induction machines and electric drives.

Pencho Vladimirov: Department of Electrical Engineering, Technical University - Sofia, 4, H. Dimitar str., 5300 Gabrovo, Bulgaria (e-mail: pvlad@iname.com)

Dimitar Spirov was born in Hisarya, Bulgaria, on May 2, 1978. He studied at the Technical University of Gabrovo-Bulgaria and received Dr. Degree from the same university in 2007.

Since 2007 he worked in the University of Food Technology - Plovdiv as a lecturer. His research interests include dynamic modes and loads and energy efficiency of the induction machines and electric drives.

Dimitar Spirov: Department of Electrical Engineering, University of Food Technologies, 26, Maritza Blvd., 4002 Plovdiv, Bulgaria (e-mail: dimitar_spirov@abv.bg)

Dynamic modes under reversing of induction machine with residual magnetic field

Dimitar Spirov, Pencho Vladimirov

Abstract: *A methodology, algorithms and mathematical models for determination of stator voltages, currents and linkage fluxes components and frequencies, rotor currents and linkage fluxes components and frequencies, electromagnetic moment and angular speed in case of induction machines with residual magnetic field reversing have been developed.*
The model investigations present that in case of induction machine with residual magnetic field reversing depending on reversing time and phase between supply voltages and electromotive force (E.M.F.) arisen from residual magnetic field, the resultant supply voltage and impact currents and moments of induction machine can be bigger than starting ones.

Keywords: *dynamic modes, induction machine, residual magnetic field, reversing*

Introduction

When switching off the induction machine stator from the mains supply the sttor windings currents decrease to zero quickly. However the induction machine magnetic flux in the event of closed rotor winding cannot decrease to zero instantly. [1,2,3] represent that a residual free currents arise in rotor windings which are opposed to the magnetic field attenuation according to the Lenz law. These currents attenuate after a time and magnetic field arouse by them is called residual magnetic field as a rule. After switching off the rotor rotation continues. Thus the residual magnetic field induces E.M.F. into stator windings which attenuate after a time also. The induction machine rotational frequency decreases under the influence of mechanical load applied to its shaft and that is why the taking into account is needed for the induced into stator windings E.M.F. frequency alteration.

In practice occur frequently cases when reversing of induction machine with residual magnetic field is necessary – for drives with intermittent duty operational mode, for stopping with reverse-switching, etc.

The analytical investigation of the residual magnetic field and thus inducted E.M.F. at constant rotational speed has been done in [1,2,3]. A transient processes investigation approach for accounting of the E.M.F. and currents caused by residual magnetic field is given in [2], over again switching on and reversing of induction machine with residual magnetic field are investigated.

All-purpose mathematical model of induction machine which can be applied for all kinds of transient processes including switching off is developed in [4]. For that purpose additional resistance R_∂ is added to the stator phase ohmic resistance R_s. The canceling of the stator currents and electromagnetic moment is going on by giving a very large value of R_∂ while $R_\partial=0$ in the rest cases. The transient processes have been investigated when switching off a three-phase induction motor with cone-shaped rotor taking into account the residual magnetic field for stages: rotation of the rotor, axial rotor travel with inductances variation and case of magnetic field killing with the purpose of breaking distance decrease.

A methodology, algorithms and mathematical models for determination of stator linkage fluxes components and frequencies, rotor linkage fluxes and currents components and frequencies, stator winding E.M.F. amplitudes and frequencies induced by the residual magnetic field in case of stopping after induction machine switching off have been developed in [5].

The aim of this paper is development of methodology, algorithms and mathematical models for determination of stator voltages, currents and linkage fluxes components and frequencies, rotor currents and linkage fluxes components and frequencies, electromagnetic moment and angular speed in case of induction machine with residual magnetic field reversing. It is necessary to obtain the induction machine operating characteristics for the dynamic modes in case of its reversing.

Mathematical model

With a view to the opportunity for investigation of the induction machine operational characteristics in case of dynamic, as well as steady-state modes, it is convenient to use the representing vectors differential equations. The development of the mathematical models and investigations have been carried out in accordance with the generally accepted admissions and symbols [6], while the iron losses have been not taken into consideration.

The three-phase induction machine dynamic stage is described by means of six equations for electric balance in the windings circuits and equation for electromechanical transforming of energy. The equations for winding voltages can be written in vector-matrix form as follows [7]

$$\mathbf{u}_{3\phi} = \mathbf{R}_{3\phi}\mathbf{i}_{3\phi} + \mathbf{L}_{3\phi}\frac{d\mathbf{i}_{3\phi}}{dt} + \omega_r \frac{d\mathbf{L}_{3\phi}}{d\varphi_r}\mathbf{i}_{3\phi}, \quad (1)$$

where φ_r and ω_r are rotational angle and angular speed of the rotor, respectively $(d\varphi_r/dt=\omega_r)$;

$$\mathbf{u}_{3\phi} = [u_{sa} \quad u_{sb} \quad u_{sc} \quad u_{ra} \quad u_{rb} \quad u_{rc}]^T;$$

$$\mathbf{i}_{3\phi} = [i_{sa} \quad i_{sb} \quad i_{sc} \quad i_{ra} \quad i_{rb} \quad i_{rc}]^T;$$

$$\mathbf{R_{3\phi}} = \begin{bmatrix} R_{sa} & 0 & 0 & 0 & 0 & 0 \\ 0 & R_{sb} & 0 & 0 & 0 & 0 \\ 0 & 0 & R_{sc} & 0 & 0 & 0 \\ 0 & 0 & 0 & R_{ra} & 0 & 0 \\ 0 & 0 & 0 & 0 & R_{rb} & 0 \\ 0 & 0 & 0 & 0 & 0 & R_{rc} \end{bmatrix};$$

$$\mathbf{L_{3\phi}} = \begin{bmatrix} L_{sasa} & L_{sasb} & L_{sasc} & L_{sara} & L_{sarb} & L_{sarc} \\ L_{sbsa} & L_{sbsb} & L_{sbsc} & L_{sbra} & L_{sbrb} & L_{sbrc} \\ L_{scsa} & L_{scsb} & L_{s\,csc} & L_{scra} & L_{scrb} & L_{scrc} \\ L_{rasa} & L_{rasb} & L_{rasc} & L_{rara} & L_{rarb} & L_{rarc} \\ L_{rbsa} & L_{rbsb} & L_{rbsc} & L_{rbra} & L_{rbrb} & L_{rbrc} \\ L_{rcsa} & L_{rcsb} & L_{r\,csc} & L_{rcra} & L_{rcrb} & L_{rcrc} \end{bmatrix}.$$

The values of windings ohmic resistances and inductances are given in Appendix 1.

The transitory value of motor electromagnetic moment is obtained to be [7]

$$M = -p_p(2/3)L_m[\,(i_{sa}i_{ra} + i_{sb}i_{rb} + i_{sc}i_{rc})\sin\varphi_r + (i_{sa}i_{rc} + i_{sb}i_{ra} + i_{sc}i_{rb})\sin(\varphi_r - 2\pi/3) + (i_{sa}i_{rb} + i_{sb}i_{rc} + i_{sc}i_{ra})\sin(\varphi_r + 2\pi/3)\,]. \quad (2)$$

The mechanical equipment is presented by one-mass dynamic model that being the case the equation of motion comes out to

$$\frac{d\omega_r}{dt} = \frac{p_p}{J_\Sigma}(M - M_c). \quad (3)$$

where M is the induction machine electromagnetic moment;

M_c – resisting moment of the mechanism;

$J_\Sigma = FI.J_m$ – total inertia moment of the machine J_m and mechanism mechanical part which is adjusted to the induction machine shaft;

FI – inertia coefficient;

ω_r – electrical angular speed of the rotor;

p_p – number of the induction machine pole pairs.

The stator phase voltages can be determine as follows

$$u_{sA} = \sqrt{2}U_N\cos(\omega_s t + \varphi_0);$$
$$u_{sB} = \sqrt{2}U_N\cos[\omega_s t + \varphi_0 - (2\pi/3)]; \quad (4)$$
$$u_{sC} = \sqrt{2}U_N\cos[\omega_s t + \varphi_0 - (4\pi/3)],$$

where ω_s is the angular frequency, φ_0 is the initial phase of the supply voltage.

Since the electric motor has got a squirrel cage rotor $u_{ra}=0$, $u_{rb}=0$ and $u_{rc}=0$.

In the presence of saturation ignoring there is an exponential pattern of the rotor currents attenuation and according to the rotor current it can be written [1]:

$$i_r = I_{r1}e^{-\frac{t}{T_{R0}}}. \quad (5)$$

The rotor currents are attenuating aperiodic currents with time constant T_{R0} and their resultant magneto-motive force is motionless according the rotor.

The currents flow through the rotor winding $\mathbf{i_r}$ excite the following linkage flux in the stator winding:

$$\psi_s = L_s i_s + L_m i_r = L_m i_r = L_m I_{r1}e^{-\frac{t}{T_{R0}}} = \frac{L_m}{L_r}\Psi_{r0}e^{-\frac{t}{T_{R0}}}. \quad (6)$$

The rotor rotates with electrical angular speed ω_r according to motionless coordinate system and the full magnetic linkage flux is

$$\boldsymbol{\Psi_s} = \frac{L_m}{L_r}\Psi_{r0}e^{-\frac{t}{T_{R0}}}e^{j\omega_r t} = \Psi_s\cos\omega_r t + j\Psi_s\sin\omega_r t = \Psi_{s\alpha} + j\Psi_{s\beta}, \quad (7)$$

where $T_{R0}=L_r/R_r$ is a time constant, corresponding to ideal idle running when supplying the rotor [1].

ω_r is obtained from the equation of motion (3).

For the inducted E.M.F. components e_{s0} caused by the rotor residual magnetic field components is obtained

$$e_{s\alpha 0} = -\frac{d\psi_{s\alpha}}{dt};\ e_{s\beta 0} = -\frac{d\psi_{s\beta}}{dt}. \quad (8)$$

In order to determine the currents in the induction machine windings in case of over again switching over from one speed to another that's sufficient to use two circuits given in [2]. The first one represents the residual rotor currents i_{rd} and i_{rq}. In order that represent them in coordinate system a,b,c immovably bound up to the rotor the following equations can be used [7]:

$$i_{ra} = i_{sd};$$
$$i_{rb} = -\frac{1}{2}i_{rd} + \frac{\sqrt{3}}{2}i_{rq}; \quad (9)$$
$$i_{rc} = -\frac{1}{2}i_{rd} - \frac{\sqrt{3}}{2}i_{rq}.$$

The second circuit defines the currents obtained as a result of stator windings resultant voltages attenuation which are equal to the sums of the mains voltages and E.M.F. from the residual magnetic field without current presence in the windings

$$u_{sAp} = u_{sA} + e_{sA0};$$
$$u_{sBp} = u_{sB} + e_{sB0}; \quad (10)$$
$$u_{sCp} = u_{sC} + e_{sC0},$$

where

$$e_{sA} = e_{s\alpha};$$
$$e_{sB} = -\frac{1}{2}e_{s\alpha} + \frac{\sqrt{3}}{2}e_{s\beta}; \quad (11)$$
$$e_{sC} = -\frac{1}{2}e_{s\alpha} - \frac{\sqrt{3}}{2}e_{s\beta}.$$

The stator and rotor currents of the supply circuit considered are marked $\mathbf{i_s^\Sigma}$ and $\mathbf{i_r^\Sigma}$ respectively.

The electromechanical processes under induction machine over again switching on in case of residual magnetic field will be represented by means of model where the following currents flow through the windings

$$\mathbf{i_s} = \mathbf{i_s^\Sigma};\ \mathbf{i_r} = \mathbf{i_r^\Sigma} + \mathbf{i_{r0}}. \quad (12)$$

The currents $\mathbf{i_s^{\Sigma}}$ and $\mathbf{i_r^{\Sigma}}$ are determined as well as the process of induction machine switching on to the voltages $u_{s\alpha p}$ and $u_{s\beta p}$ is considered and an admittance that the magnetic field is attenuated.

By $\mathbf{i_{r0}}$ is marked the current which flows through the rotor windings until the induction machine over again switching on to the mains and it is defined from the machine previous mode of operation.

The software package MATHCAD has been used for solving a systems of differential equations obtained and transformed in the *Cauchy*-form [8].

Results obtained

By means of the methodology, algorithms and mathematical models developed the dynamic modes under switching on and reversing of induction motor type T100 LB-4 in case of rated load $M_c=M_N=const.$ have been investigated. The technical data of the electric motor are given in Appendix 2. The T-shape equivalent circuit of the motor parameters determinate by a firm-producer calculating methodology accordingly different values of the slip are given in Appendix 3. The inertia coefficient $FI=2,0$ is assumed.

After switching on of the induction machine and reaching to steady-state speed a time $t_1=0,5s$ later the mains supply is switching off and a reversing carries out by two of the supply phases transposing: applying the voltage u_{sB} to phase A winding where a residual magnetic field is presented; applying the voltage u_{sA} to phase B winding where a residual magnetic field is presented; applying the voltage u_{sC} to phase C winding where a residual magnetic field is presented;

By means of the mathematical models the dependencies of motor developed operational characteristics in case of dynamic and steady-state modes under reversing have been obtained. Some of the results obtained are presented on the respective figures.

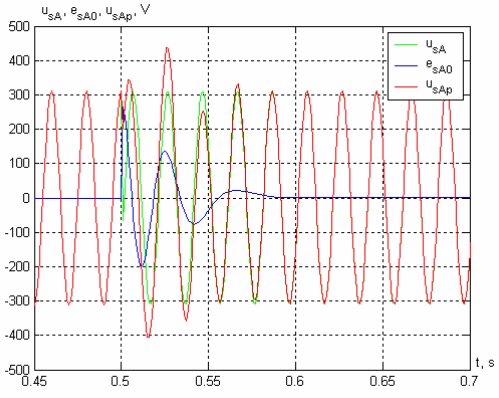

Fig. 1. Dependencies u_{sA}, e_{sA0}, $u_{sAp}=f(t)$

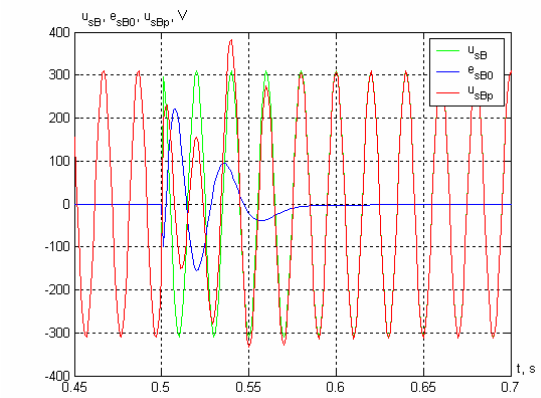

Fig. 2. Dependencies u_{sB}, e_{sB0}, $u_{sBp}=f(t)$

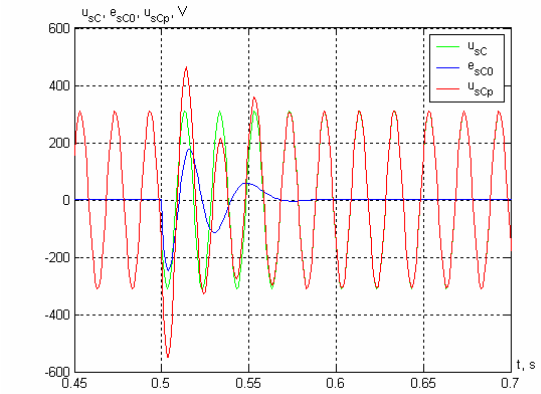

Fig. 3. Dependencies u_{sC}, e_{sC0}, $u_{sCp}=f(t)$

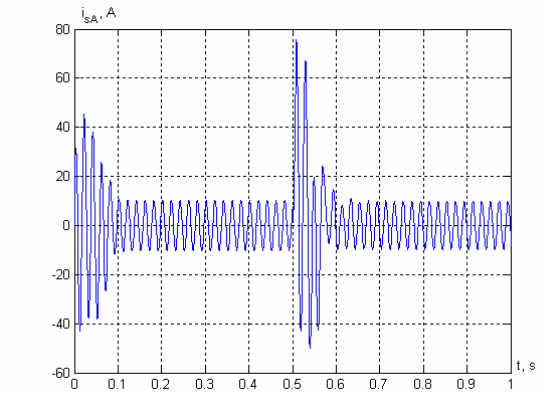

Fig. 4. Dependence $i_{sA}=f(t)$

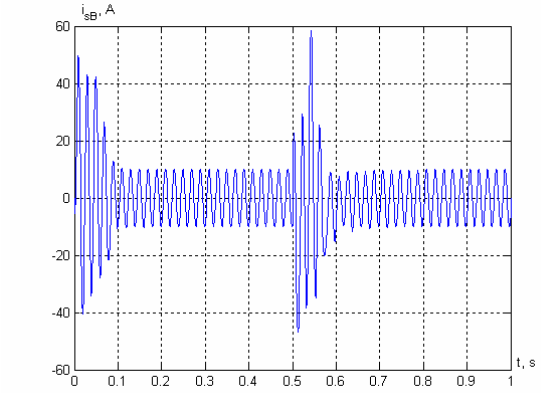

Fig. 5. Dependence $i_{sB}=f(t)$

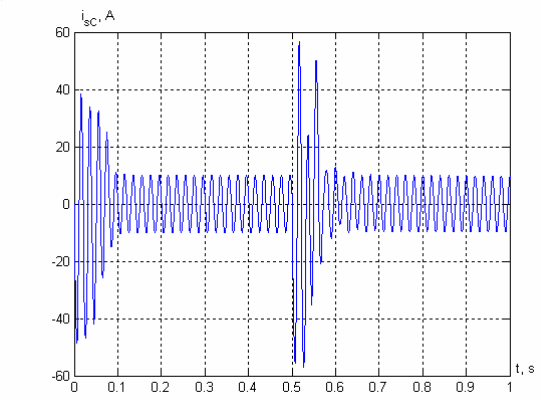

Fig. 6. Dependence $i_{sC}=f(t)$

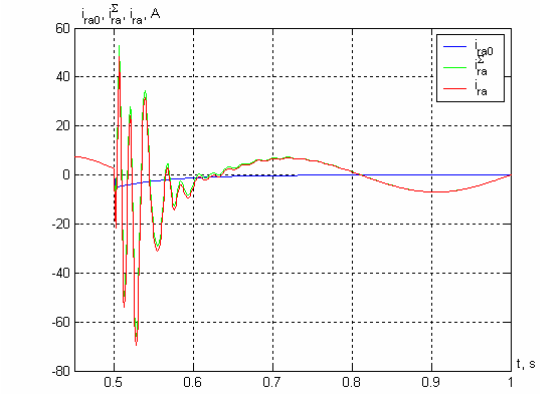

Fig. 7. Dependencies i_{rA0}, i_{rA}^{Σ}, $i_{rA}=f(t)$

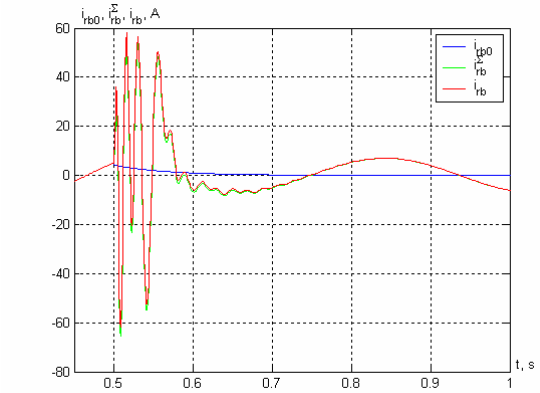

Fig. 8. Dependencies i_{rB0}, i_{rB}^{Σ}, $i_{rB}=f(t)$

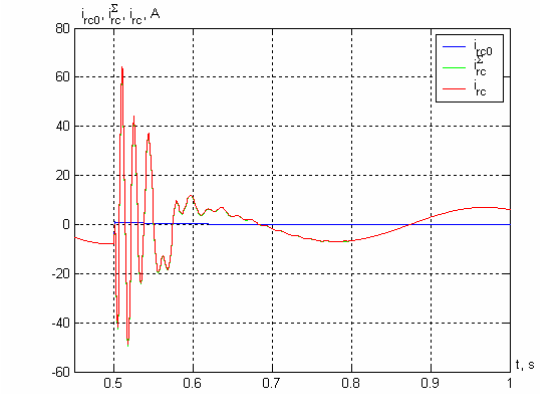

Fig. 9. Dependencies i_{rC0}, i_{rC}^{Σ}, $i_{rC}=f(t)$

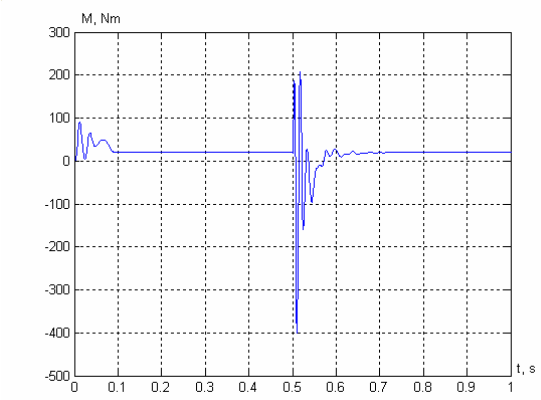

Fig. 10. Dependence $M=f(t)$

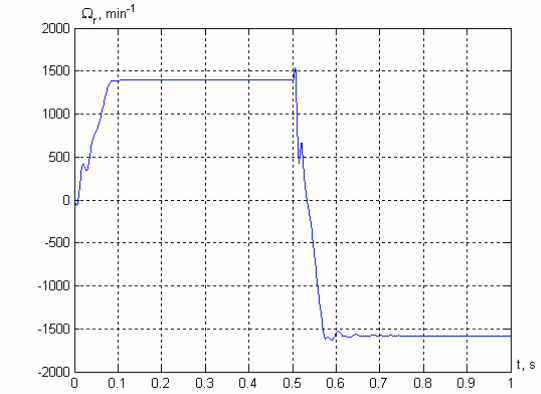

Fig. 11. Dependence $\Omega_r=f(t)$

Table 1 represents the values of U_{spmax}, $i_{y\partial}$, $M_{y\partial}$ under switching on and reversing of induction machine with residual magnetic field.

Table 1

Table 1. Values of U_{spmax}, $i_{y\partial}$, $M_{y\partial}$ in cases of starting and reversing.

	Starting	Reversing		
		Phase A	Phase B	Phase C
U_{spmax}, V	311,127	436,538	383,648	550,795
$i_{y\partial}$, A	45,559	75,539	58,429	56,961
$M_{y\partial}$, Nm	90,491	400,528		

From Table 1 it can be seen that under reversing of induction machine with residual magnetic field the maximum value of the resultant supply voltage can reach value twice greater than rated one. By reason of this the impact currents and moments increase and they can be greater than starting ones.

Conclusion

The methodology, algorithms and mathematical models developed allow the determination of stator voltages, currents and linkage fluxes components and frequencies, electromagnetic moment and angular speed in case of induction machine with residual magnetic field reversing.

The model investigations pointed out that in case of induction machine with residual magnetic field reversing

the resultant supply voltage and impact currents and moments can be greater than starting ones.

Appendix 1

Values of ohmic resistances and inductances

$R_{sa}=R_{sb}=R_{sc}=R_s$; $R_{ra}=R_{rb}=R_{rc}=R_r$;
$L_{sasa}=L_{sbsb}=L_{scsc}=L_{\sigma s}$; $L_{rara}=L_{rbrb}=L_{rcrc}=L_{\sigma r}$;
$L_{sasb}=L_{sasc}=L_{sbsa}=L_{sbsc}=L_{scsa}=L_{scsb}=-L_m$;
$L_{rarb}=L_{rarc}=L_{rbra}=L_{rbrc}=L_{rcra}=L_{rcrb}=-L_m$;
$L_{sara}=L_{sbrb}=L_{scrc}=L_{rasa}=L_{rbsb}=L_{rcsc}=(2/3)L_m\cos\varphi_r$;
$L_{sarc}=L_{sbra}=L_{scrb}=L_{rcsa}=L_{rasb}=L_{rbsc}=(2/3)L_m\cos(\varphi_r-2\pi/3)$;
$L_{sarb}=L_{sbrc}=L_{scra}=L_{rbsa}=L_{rcsb}=L_{rasc}=(2/3)L_m\cos(\varphi_r+2\pi/3)$;
$L_{\sigma s}=X_{\sigma s}/\omega_s$; $L_{\sigma r}=X_{\sigma r}/\omega_s$; $L_m=X_m/\omega_s$.

Appendix 2

Technical data of induction motor type T100 LB-4

$P_N=3{,}00kW$; $U_N=220V$; $I_N=6{,}8A$; $f=50Hz$; $p_p=2$; $n_N=1406{,}3min^{-1}$; $s_N=0{,}0624$; $M_N=20{,}434Nm$; $J_m=0{,}00619kg.m^2$.

Appendix 3

Parameters of induction motor type T100 LB-4

Slip	R_s, Ω	R_r, Ω	$X_{\sigma s}$, Ω	$X_{\sigma r}$, Ω	X_m, Ω
$s=0{,}0017$	2,258	2,329	2,488	2,949	34,48
$s=0{,}06$	2,318	2,329	2,602	3,029	46,82
$s=1{,}0$	2,318	2,393	2,084	2,301	46,82

References

[1] Kovacs, K. P., I. Racz. Transient processes in AC machines. Moscow, Gosenergoizdat, 1963, p. 744. (in Russian)

[2] Sokolov, M. M., L. P. Petrov, L. B. Masandilov, V. A. Ladenzon. Electromagnetic transient processes in induction machine drive. Moscow, Energia, 1967, p. 201. (in Russian)

[3] Dinov V. R., Non-symetrical modes and transient processes in electric machines. Tehnika, Sofia, 1974, p. 370. (in Bulgarian)

[4] Dinov V., E. Sokolov. Transient process under switching off the three-phase induction motor with cone-shaped rotor. Annals of Technical University - Sofia, 1974. (in Russian)

[5] Vladimirov, P. Investigation of transient processes and residual magnetic field in case of induction machines stopping. „Electrotechnics and electronics", №3-4, 2006, pp. 69-76. (in Bulgarian)

[6] Kopilov I. P. Mathematical modeling of electric machines. Moscow, Vissha shkola, 2001, p. 327. (in Russian)

[7] Spirov D. Energy-efficient speed alteration of induction machines by means of magnetic field orientation. PhD Thesis, Gabrovo, 2007.

[8] MathCad Electronic Book – The MathSoft Electronic Book Samlper. 1994, MathSoft Inc.

Biographies

Dimitar Spirov was born in Hisarya, Bulgaria, on May 2, 1978. He studied at the Technical University of Gabrovo-Bulgaria and received Dr. Degree from the same university in 2007.

Since 2007 he worked in the University of Food Technology - Plovdiv as a lecturer. His research interests include dynamic modes and loads and energy efficiency of the induction machines and electric drives.

Dimitar Spirov: Department of Electrical Engineering, University of Food Technologies, 26, Maritza Blvd., 4002 Plovdiv, Bulgaria (e-mail: dimitar_spirov@abv.bg)

Pencho Vladimirov was born in village Gorna Lipnitza, province V.Tarnovo, Bulgaria, on December 2, 1942. He studied at the Technical University of Sofia - Bulgaria and graduated in 1968. He received the PhD degree and DSc degree, in 1978 and 2008, respectively.

Since 1970 he worked in the Technical University - Gabrovo as a lecturer. In 1982, he was elected Assoc. Prof. in Electrical Machines. His research interests include dynamic modes and loads and energy efficiency of the induction machines and electric drives.

Pencho Vladimirov: Department of Electrical Engineering, Technical University - Sofia, 4, H. Dimitar str., 5300 Gabrovo, Bulgaria (e-mail: pvlad@iname.com)

Reseach on dynamics of the movement of the charged particles

Penka N. Miteva, Atanas K. Ivanov

Abstract: *The following article deals with the dynamics of the movement of the charged particles in electrostatic field of the dielectric material phosphorite which is used in the production of mineral fertilizers. The FDL (electrostatic force) is investigated. It is determined according to the method of mirror images. When compared to the force of weight F_T of separated particles with certain size it is proved to what an extent the electrostatic force can be used to attract the particles to the electrode.*

Keywords: *dielectric penetrability, phosphorite, charged particle*

Introduction

The present publication is a continuation of investigations, dealing with the problem of the electrostatic separation of materials with different dielectric penetrability.. The calculation presented in the form of tables and graphics prove that the power of the mirror image is not strong enough to bring the particle to the electrode. By determining the Qulonic force between the charge of the particle q and the intensity of the electrostatic field E, the resultant force is strong enough to bring the particle into movement. With the help of this investigation, conclusions are made about the process of separation of particles with certain measures, when the values of voltage applied and the distance between the electrodes are varied.

Exposition

It is shown the movement of charged particle between two electrodes of surface – circumference type. With the help of programming product FEMM [3,5] there is a picture given of the electrostatic field with same electrode configuration and the value of field intensity E. The type of electrodes and the field picture concerning electrode distance 0.005m and 0.1 m are shown on fig. 1 (a, b, c).

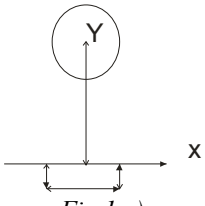

Fig.1.a)

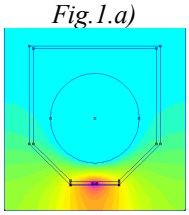

Fig.1.b) electrode distance 0.005m

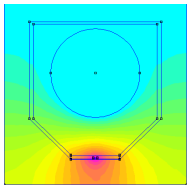

Fig.1.c) electrode distance 0.1m

What is shown is the movement of a sphere particle with radius a, which falls in the zone of коронния discharge and gains certain charge $q_{диел}$ determined by dielectic penetrability ε_r and intensity of the field E in a given position. To determine the charge $q_{диел}$ we can use the dependence.

$$(1) \quad q_{диел} = 4.\pi.\varepsilon_0.(1+2.\frac{\varepsilon_r - 1}{\varepsilon_r + 2}).a^2.E$$

As:

ε_0 = 8,85.10-12, F/m; E – intensity, taken by the modified field picture, V/m.

The movement of a phosphorite particle is being shown, for which according to technological requirements radius a = $0{,}04.10^{-3}$ m [4] and has relative dielectrical penetrability ε_r =8,32, indicated by digital capacity measuring device ESCORT ELC-1310.

By substituting in (1) for the charge of this particle we get the dependence:

$$(1') \quad q_{ф.} = 4.3{,}14.8{,}85.10^{-12}.(1+2.\frac{8{,}32-1}{8{,}32+2}).(0{,}04.10^{-3})^2.E = 0{,}43.10^{-18}.E$$

We take that the precipitating flat electrode is a metal and its dielectrical penetrability is $\varepsilon_м = \infty$ [2].

By the разликата in dielectrical penetrability of the air $\varepsilon_в$ =1 and the metal according the mirror images method we can determine the force $F_{диел}$ of attraction of the charged particle towards the circumference. This force is calculated with the following formula [2]:

$$(2) \quad F_{диел.} = -\frac{q^2_{диел.}}{4.\pi.\varepsilon_0.4.z^2}$$

as z is the distance to the surface of the circumference along the y axis.

The weight of the particle can be determined through the equation:

$$(3) \quad F_T = m_p.g = \sigma.V.g = 2{,}5.10^3.9{,}8.2{,}679.10^{13}.9{,}81 = 6{,}44.10^{-8}\,N$$

as we know:

σ =$2{,}5.10^3$kg/m^3=$2{,}5.10^3$.9,8 N/m^3 – weight of the phosphorite,

$$(4) V = \frac{4}{3}\pi.a^3 = \frac{4}{3}.3{,}14.(0{,}04.10^{-3})^3 = 2{,}679.10^{-13}, m^3$$

m_p - mass of the particle g – gravitation; V – volume of the particle.

In table 1.[3] we have been given the results depending on the distance 0.05m between the electrodes concerning intensity E, determined charge $q_{диел}$ and the force of the mirror image $F_{диел}$ in case U_1=50kV and U_1=50kV.

According to fig.1 and the taken coordinates system the distance between the corona electrode and the drum is z_1.

Analogically we have the results on table 2 [3] for a distance of 0.1m and U_1=50kV и U_2=100kV and the distance is z_2.

z_1= 0.05 – y and z_2= 0.1 – y.

At fig. 5, 6 , 7 the following dependences are shown E=f(z_2), $q_{диел}$=f(z_2), $F_{диел}$=f(z_2), accounted form table 2.

Table 1

	0.05m U_1=50kV		
z_1,[m]	**E_z,[v/m]**	**Q_{diel}[Q]**	**$F_{diel.}$[N]**
0	$2{,}156.10^{6}$	$0{,}927.10^{-12}$	$-0{,}00008.10^{-8}$
0.01	$1{,}171.10^{6}$	$0{,}503.10^{-12}$	$-0{,}00012.10^{-8}$
0.02	$0{,}848.10^{6}$	$0{,}363.10^{-12}$	$-0{,}00021.10^{-8}$
0.03	$0{,}717.10^{6}$	$0{,}308.10^{-12}$	$-0{,}00048.10^{-8}$
0.04	$0{,}617.10^{6}$	$0{,}265.10^{-12}$	$-0{,}0019.10^{-8}$
0.05	$0{,}600.10^{6}$	$0{,}282.10^{-12}$	$-29{,}49.10^{-8}$
	0.05m U_2=100kV		
z_1,[m]	**E_z,[v/m]**	**Q_{diel}[v/m]**	**F_{diel}[v/m]**
0	$4{,}313.10^{6}$	$1{,}85.10^{-12}$	$-0{,}0003.10^{-8}$
0.01	$2{,}382.10^{6}$	$1{,}02.10^{-12}$	$-0{,}00048.10^{-8}$
0.02	$1{,}687.10^{6}$	$0{,}725.10^{-12}$	$-0{,}00086.10^{-8}$
0.03	$1{,}43.10^{6}$	$0{,}614.10^{-12}$	$-0{,}0019.10^{-8}$
0.04	$1{,}343.10^{6}$	$0{,}577.10^{-12}$	$-0{,}0077.10^{-8}$
0.05	$1{,}314.10^{6}$	$0{,}500.10^{-12}$	$-120{,}79.10^{-8}$

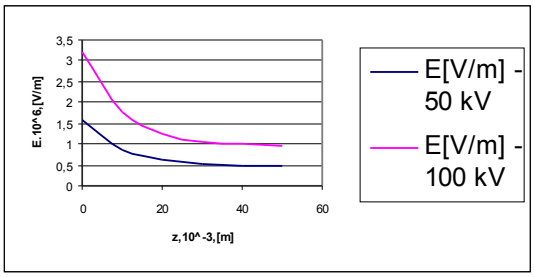

Fig.2. At fig. 2 the following dependences are shown E=f(z_1) accounted from table 1.

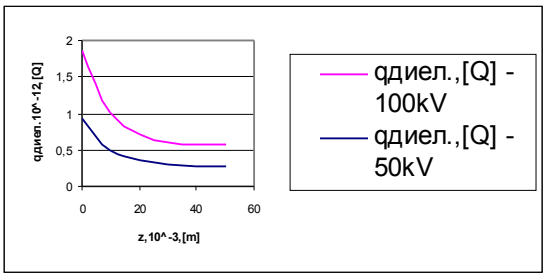

Fig.3.At fig. 3 the following dependences are shown $q_{диел}$=f(z_1) accounted from table 1.

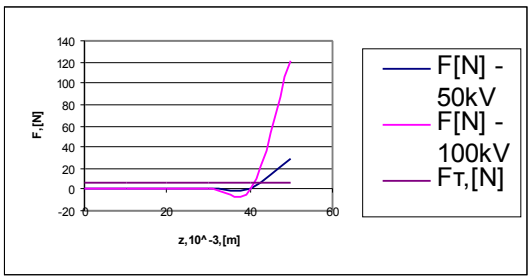

Fig.4.At fig.4 the following dependences are shown $F_{диел}$=f(z_1), accounted from table 1.

Table 2

	0.1m U_1=50kV		
z_2,[m]	**E_z,[v/m]**	**$q_{диел.}$[Q]**	**$F_{диел.}$[N]**
0	$1{,}579.10^{6}$	$0{,}679.10^{-12}$	$-0{,}00001.10^{-8}$
0.01	$0{,}899.10^{6}$	$0{,}386.10^{-12}$	$-0{,}00001.10^{-8}$
0.02	$0{,}581.10^{6}$	$0{,}25.10^{-12}$	$-0{,}00002.10^{-8}$
0.03	$0{,}445.10^{6}$	$0{,}192.10^{-12}$	$-0{,}00002.10^{-8}$
0.04	$0{,}395.10^{6}$	$0{,}17.10^{-12}$	$-0{,}00003.10^{-8}$
0.05	$0{,}358.10^{6}$	$0{,}154.10^{-12}$	$-0{,}00004.10^{-8}$
0.06	$0{,}336.10^{6}$	$0{,}145.10^{-12}$	$-0{,}00006.10^{-8}$
0.07	$0{,}325.10^{6}$	$0{,}139.10^{-12}$	$-0{,}00011.10^{-8}$
0.08	$0{,}324.10^{6}$	$0{,}139.10^{-12}$	$-0{,}00025.10^{-8}$
0.09	$0{,}325.10^{6}$	$0{,}139.10^{-12}$	$-0{,}0010.10^{-8}$
0.1	$0{,}100.10^{6}$	$0{,}043.10^{-12}$	$-16{,}19.10^{-8}$
	0.1m U_2=100kV		
z_2,[m]	**E_z,[v/m]**	**$q_{диел.}$[Q]**	**$F_{диел.}$[N]**
0	$1{,}879.10^{6}$	$0{,}808.10^{-12}$	$-0{,}00001.10^{-8}$
0.01	$1{,}797.10^{6}$	$0{,}773.10^{-12}$	$-0{,}00002.10^{-8}$
0.02	$1{,}666.10^{6}$	$0{,}716.10^{-12}$	$-0{,}00002.10^{-8}$
0.03	$0{,}887.10^{6}$	$0{,}339.10^{-12}$	$-0{,}00003.10^{-8}$
0.04	$0{,}788.10^{6}$	$0{,}308.10^{-12}$	$-0{,}00004.10^{-8}$
0.05	$0{,}717.10^{6}$	$0{,}289.10^{-12}$	$-0{,}00006.10^{-8}$
0.06	$0{,}672.10^{6}$	$0{,}280.10^{-12}$	$-0{,}00009.10^{-8}$
0.07	$0{,}651.10^{6}$	$0{,}279.10^{-12}$	$-0{,}00017.10^{-8}$
0.08	$0{,}649.10^{6}$	$0{,}280.10^{-12}$	$-0{,}00038.10^{-8}$
0.09	$0{,}650.10^{6}$	$0{,}276.10^{-12}$	$-0{,}0015.10^{-8}$
0.1	$0{,}641.10^{6}$	$0{,}040.10^{-12}$	$-22{,}92.10^{-8}$

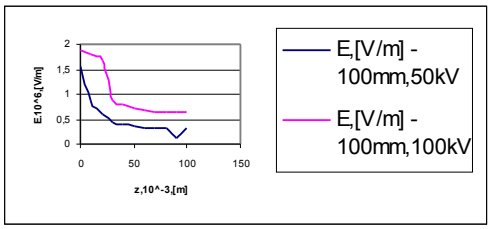

Fig.5. At fig. 5 the following dependences are shown E=f(z_2) accounted form table 2.

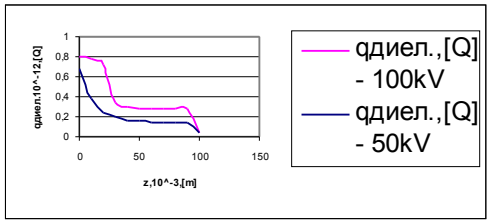

Fig.6. At fig. 6 the following dependences are shown E=f(z_2), $q_{диел}$=f(z_2), $F_{диел}$=f(z_2), accounted form table 2.

Table 4

	z_2=0.1–y, [m]	0.1	0.09	0.08	0.07	0.06
50kV	$F_k.10^{-6}$	1.072	0.61	0.394	0.302	0.268
100kV	[N]	1.518	1.452	1.346	0.717	0.637
	z_2=0.1–y, [m]	0.05	0.04	0.03	0.02	0.01
50kV	$F_k.10^{-6}$	0.243	0.228	0.221	0.219	0.219
100kV	[N]	0.579	0.543	0.526	0.524	0.525

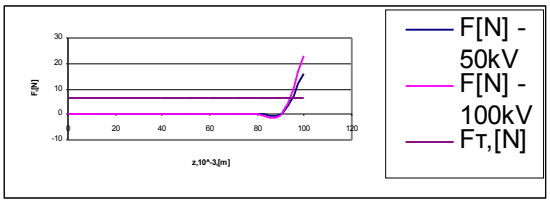

Fig.7.At fig.7 the following dependences are shown F=f(z), accounted form table 2.

The force of the mirror image is not enough by itself to move the particle towards the precipitating flat drum. Here it has to be taken into account the Qulonic force, that is resulted from the cooperation of the charge $q_{диел}$ of the particle and the intensity E of the electrostatic field. It is determined by the following dependence:

$$(5)\quad F_k = q.E = 4.\pi.\varepsilon_0.a^2.E.(1+2.\frac{\varepsilon_r - 1}{\varepsilon_r + 2}).E_z$$

At table 3. [3] we have the results given in dependence of the distance z_1=0.05–y between the Qulonic force electrodes F_k at rates U_1=50kV и U_2=100kV.

At table 4. [3] we have given the results in relation of the distance z_2=0.1–y between the Qulonic force electrodes F_k at rates U_1=50kV и U_2=100kV.

Tabl e 3

	z_1=0.05–y, [m]	0.05	0.04	0.03	0.02	0.01	0.005
U_1=50 kV	$F_k.10^{-6}$ [N]	2	1.09	0.79	0.67	0.57	0.56
U_2=100kV		7.98	4.41	3.12	2.65	2.49	2.41

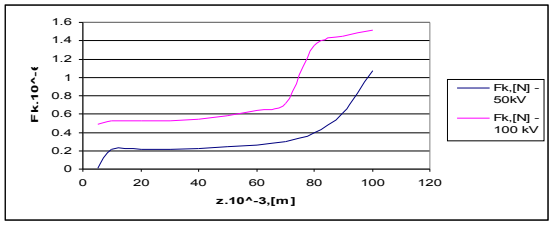

Fig.8.At figure 8 the following dependence is presented F_k =f(z_1), calculate from table 3.

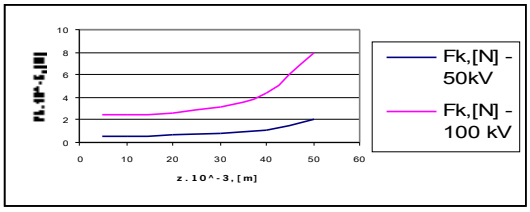

Fig.9. At figure 9 the following dependence is presented F_k =f(z_2), calculate from table 4

Conclusion

1. The force of the mirror image is not enough to move the particle towards the precipitating flat drum.
2. For a distance z=0.05m the attraction force of the mirror image is bigger than the weight force after 10 mm from the drum surface.
3. For a distance of z=0.1 m the attraction force is bigger than the weight force after 0.005m from the drum surface.
4. In order to get to the process of sticking of the particles, additional force is needed to move them to the zone of possible attraction from the electrostatic force of the mirror image.
5. The determined кулонова force F_k is considered enough when at the given pressures, the phosphorite particle with a radius a = 0,04.10-3 m can overcome the weight force $F_т$ and to reach the precipitating flat electrode.

References:

1. Bolotov, V., Sh, T.A., Elektrotehnologie storage, S. Petemburg, 1989;
2. Penchev, P., Electrotehnolagie, Sofia – 1983;
3. Miteva, P., Ivanov A. , Research work determining the influence of the dielectric penetrability of the separated material on the distribution of the electric field, XV-th Internacional symposium on Electrical Apparatus and Technologies, SIELA 2007, 31 may – 1 juni 2007, Plovdiv, Bulgaria;
4. Programming product FEMM, David Mecker, 2003; http://femm.berlios.de;
5.Electrical guide, Moskva, Energoatomizdat 1988

Biographies

Professor engineer Atanas Ivanov, professor at Varna Technical University, Faculty of Electronics. Working in the sphere of electro technologies.(ativ@abv.bg)

Master engineer Penka N. Miteva, doctorant at Varna Technical University, Faculty of Electronics, profile: "Electrotechnics and Electrical Technologies". Graduated 2005 in "Electrotechnics" profile. Working in the sphere of electro separation.(p_nedkova@abv.bg)